




Review

Challenges and Future Prospects of the MXene-Based Materials for Energy Storage Applications

Svitlana Nahirniak , Apurba Ray  and Bilge Saruhan * 

German Aerospace Center, Institute of Materials Research, Linder Hoehe, 51147 Cologne, Germany

* Correspondence: bilge.saruhan@dlr.de

Abstract: In the past decade, MXenes, a new class of advanced functional 2D nanomaterials, have emerged among numerous types of electrode materials for electrochemical energy storage devices. MXene and their composites have opened up an interesting new opportunity in the field of functional materials, owing to their transition metal nitrides/carbides/carbonitride-based unique layered structures, higher electrical and thermal conductivity, higher charge carrier mobility, high negative zeta-potential, high mechanical properties, tunable bandgap, superior hydrophilicity, metallic nature and rich surface chemistry, which enhance the number of metal active redox sites on the surface and short ion diffusion path. However, in the case of electrochemical energy storage applications, the unavoidable problem of aggregation and nanosheet restacking significantly reduces the accessibility of the active surface sites of MXene materials for electrolyte ions. Currently, there is a number of research efforts devoted to solutions in order to avoid these deficits. This Review complies extensively with the recent advances in the application of MXene-based materials in the energy storage devices such as batteries and supercapacitors. Particular attention is paid to the understanding of the relation of MXenes chemical composition, and morphology with their electrochemical performances. Moreover, the challenges of MXenes and MXene-based composited for the commercial application are considered and the ways to overcome their drawbacks are provided. Finally, opportunities given with MXenes for future research on novel energy storage materials are highlighted.

Keywords: MXenes; electrochemical energy storage; supercapacitors; batteries; 2D layered structures



Citation: Nahirniak, S.; Ray, A.; Saruhan, B. Challenges and Future Prospects of the MXene-Based Materials for Energy Storage Applications. *Batteries* **2023**, *9*, 126. <https://doi.org/10.3390/batteries9020126>

Academic Editor: Chuang Yu

Received: 29 December 2022

Revised: 30 January 2023

Accepted: 7 February 2023

Published: 10 February 2023



Copyright: © 2023 by the authors. Licensee MDPI, Basel, Switzerland. This article is an open access article distributed under the terms and conditions of the Creative Commons Attribution (CC BY) license (<https://creativecommons.org/licenses/by/4.0/>).

1. Introduction

The next generation of electrochemical storage devices demands improved electrochemical performance, including higher energy and power density and long-term stability [1]. As the outcome of electrochemical storage devices depends directly on the properties of electrode materials, numerous researchers have been developing advanced materials and hybrid composites [2]. For instance, it is well known that the good contact between electrode and electrolyte, as well as stable long-term cycling, depends directly on the materials' morphology, which may be controlled via synthesis approach and processing conditions (e.g., precursors, reaction parameters, synthesis type). Specific architectures and nanodimensional structures have proved themselves to exhibit better electrochemical performance compared to their bulk counterparts, resulting in faster ion transport and larger energy capacity. The relation between morphological characteristics and materials' application in energy storage devices, and particularly the analysis of factors affecting the morphology and structure of electrode materials, has been comprehensively studied in [3]. In their review manuscript, Hussain et al. [4] have highlighted the importance of the morphology of nanostructures for surface engineering and, thus, electrode designing. Authors have demonstrated that nanostructures with nature-inspired morphologies (coral-like, urchin-like, sea sponge-like, snowflake-like, etc.) possess high surface area and increased number of redox-active sites, providing beneficial advantages in electrochemical energy storage applications. Despite the excellent physical and chemical properties of these

materials, such as shortened paths for fast lithium ion diffusion and large surfaces [5–8], the number of their drawbacks, such as poor specific capacitance, lower electrical conductivity, structure degradation and limited ions/electrons transport, force research to look for new compounds [9,10].

Li-ion batteries (LIB) were designed as clean energy storage devices, able to provide high energy density, moderate power density and life cycle stability [11]. The set of numerous advantages of the LIB is due to the set of their fundamental chemical properties. Li has the lowest potential among chemical elements and one of the smallest ionic radii of any single charged ion, resulting in the highest cell potential, high gravimetric and volumetric capacity and power density [12].

Supercapacitors (SCs) or ultracapacitors are recognized as a new class of promising electrochemical energy storage devices for next-generation energy systems [13,14]. Supercapacitors have several advantages such as rapid charge storage capability (\sim Farad), high power densities (>10 kW/kg), fast charge/discharge rates (\sim few ms), excellent cycle life (\sim 1M cycles), low cost and good safety compared with the present market-leading LIBs [15,16]. Rapid adsorption/desorption capability of electrolyte ions on the surface of the electrodes under an electric field makes supercapacitors promising for high energy storage and enables them to be widely used in different energy storage systems such as smart grid, automotive industry, renewable energy storage including wind and solar systems [3].

Porous and activated carbon (AC), graphene, carbon nanotubes (CNT) and other carbon-based materials are generally used for commercial supercapacitor fabrication. However, low volumetric performance, including low energy density (<20 mWh/cm³), low volumetric capacitance (<200 F/cm³) and lower operating voltage (<2.7 V) are major challenges in current supercapacitor research. Therefore, advanced electrode materials with higher capacity, higher voltage and energy densities are an urgent and desirable need for future supercapacitors [17–19].

Relying on their unique structure, large surface area, high electrical and thermal conductivity, fast ion diffusion, thickness and composition controllability [20], MXenes, a new class of electrode materials have attracted great attention and favourable performance in energy storage devices. Gogotsi and his co-workers in 2011 first discovered MXene as a promising member of the advanced functional 2D nanomaterials that met unprecedentedly exponential progress in batteries and supercapacitors [21,22]. In general, the common chemical structure of MXene is $M_{y+1}X_yT_x$ where M stands for transition metals, X represents C/N/C_xN_y and T indicates the terminating surface groups i.e., -OH, -O, -F, etc. Characteristically, MXenes can also be obtained through the “top-down” approach by etching A layers from the MAX phase with space group p63/mmc making large-scale 2D MXene with improved properties [23,24]. Incredible associated structures with a layered morphology, fast electron transport and rapid ion diffusion capability, intrinsic high electronic conductivity (up to $\approx 24\,000$ S/cm), hydrophilicity, favourable pseudocapacitive performance and enriched surface functionalities of MXene play a significant role in high electrochemical energy storage performance over other 2D materials [25–27]. Transport of ions and electrons at the interface is possible and the agglomeration of the active mass during intercalation/deintercalation can be avoided by monitoring the surface functionalities of MXene electrodes [2,28].

Although pure MXene exhibits better electrochemical properties, the electrodes made of MXene suffer from inherent layer restacking due to van der Waals interactions limiting its use in dense structures for commercial applications with long life. Consequently, long-term cyclic use of MXene electrodes faces deteriorations such as poor capacitance retention, lower stability, and insufficient diffusion of electrolyte ions as far as lowered cycle numbers.

The electrochemical performance of the MXene-based materials can be adjusted by a number of aspects, including interlayer distance [9], surface terminations [29], and chemical composition [30]. Current research works showed that combining other materials with MXenes to produce MXens-based composite electrode materials is one of the most effective strategies for energy storage applications [31]. Up to now, compositionally more

than 30 numbers of MXenes have been experimentally realized and their performances are reported, and, interestingly, among them, $Ti_3C_2T_x$ MXene has received the topmost attention because of the redox-active Ti atom offering high volumetric capacitance. On the other hand, the conductive carbide layer boosts the ion transport and movement of electrons towards redox-active sites.

Thus, the rational synthesis of the MXene-based materials with controlled composition, metal/carbon ratio and surface terminations can greatly improve their lithium storage performance and, as a result, their applications in lithium-ion batteries, as well as in supercapacitors [8]. Moreover, the synergetic improvement in MXene's electrochemical characteristics can be achieved by the formation of MXene-based hybrid materials. The introduction of metal oxides, silicon or carbon-based materials can not only allow us to achieve high capacitances [8], but also to avoid stacking of the MXene single layers [32].

The present review provides a summary of the recent advances in the application of MXene-based materials in energy storage devices. The previously published review papers on MXene applications in energy storage devices are mostly concentrated on the MXene synthesis approaches, their fundamental properties and electrochemical activity for their operation in different thermal fields, including not only energy storage devices, but also photovoltaic, desalination, electrocatalysis [8,9,20,28,33–35]. In comparison to that, particular attention in the present work has been paid to the understanding of the relation between MXenes chemical composition, surface terminations and morphological features with their electrochemical performance in batteries and supercapacitors. The challenges of MXenes and MXene-based composites for commercial application have been considered and the ways to overcome their drawbacks have been provided.

2. Charge Storage Mechanism in MXenes

2.1. In the Li-Ion Batteries

With respect to the charging mechanism of MXene compounds in Li-ion batteries, so far, the attention of researchers has mostly focused on the investigations of the material's surface structures. However, compositional characteristics and the effect of Li-adsorption energy as a function of Li content on the charging mechanism are other significantly crucial factors to be studied for the understanding of the Li adsorption mechanism in batteries built with MXene. In this regard, the investigations of Sun et al. on the effect of MXenes composition, their surface structure, as well as variation in Li concentration on the reaction mechanism of MXene compounds in Li-ion batteries electrodes using density functional calculations are valuable contributions [36].

According to the structural transformation during the Li adsorption, researchers and authors dealing with MXenes compound considered two main groups: V-type (V_2CO_2 , Cr_2CO_2 , and Ta_2CO_2) and Sc-type (Sc_2CO_2 , Ti_2CO_2 , Zr_2CO_2 , Nb_2CO_2 , and Hf_2CO_2). The initial molecular dynamic simulations confirmed that structural transformation in V-type MXenes is reversible during lithiation/delithiation. It has been demonstrated, that during the lithiation process in V-type compounds the formation of Li–O (M=V, Cr, Ta) bonds is preferable to the M–O bonds (M=V, Cr, Ta):



Moreover, the authors investigated the effect of surface terminations on Li intercalation (Figure 1), and have shown that Li mobility on V_2CO_2 is larger than those on V_2CF_2 and $V_2C(OH)_2$.

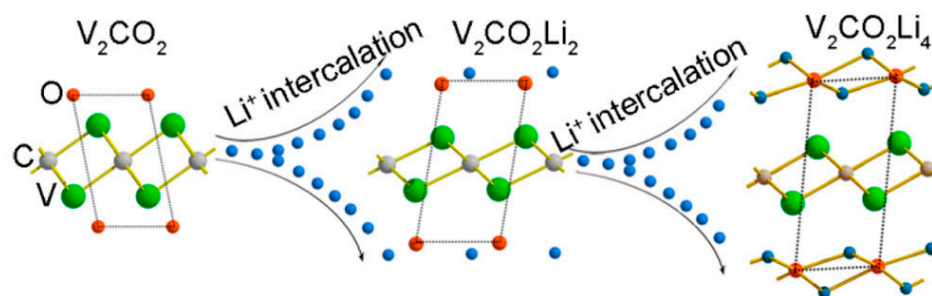


Figure 1. Schematic representation of the lithiation process in V-type (V_2CO_2 , Cr_2CO_2 , and Ta_2CO_2) MXenes. Reprinted with permission from [36]. Copyright © 2016, American Chemical Society.

2.2. In Electrode-Based Supercapacitors

In general, there are two types of charge storage mechanisms associated with supercapacitors e.g., electrical double-layer capacitors (EDLCs) and pseudo-capacitors. In the case of EDLCs, charges are accumulated at the electrode/electrolyte interface forming an electrostatic double layer. There is no electron transfer or any redox reaction occurring for EDLC, which means energy is stored in the materials by a non-Faradic process. On the other hand, in pseudo-capacitors, transfer of electrons or Faradic redox reaction occurs being mainly independent of electrode surface area [37,38]. Moreover, electrolyte ions in pseudo-capacitors transfer across the electrode to a conducting bulk phase, although electrons or ions leave the electrode after the redox reaction. On the contrary, charges that enter the electrode do not leave the electrode in the case of non-Faradic processes [39]. Atoms that are part of the electrodes contribute to the charge storage mechanism for EDLCs and can be identified from the type of cycle voltammogram (CV) curve shape. In Figure 2, the different shapes of CV and GCD curves represent the different types of charge storage mechanisms for supercapacitors [40]. MXenes possess layers providing space for charge accumulation and are rich in functional groups where redox reaction and energy storage take place within these active groups as well as at the different layers and their interfaces of MXenes. Research is ongoing in different fields of electrical energy storage devices by producing MXenes-based and electrode materials with hybrid architectures to achieve high energy density and stability of the SC electrode materials. However, there are still many unavoidable factors affecting the energy storage performance of MXenes-based electrodes which need to be definitively overcome [41].

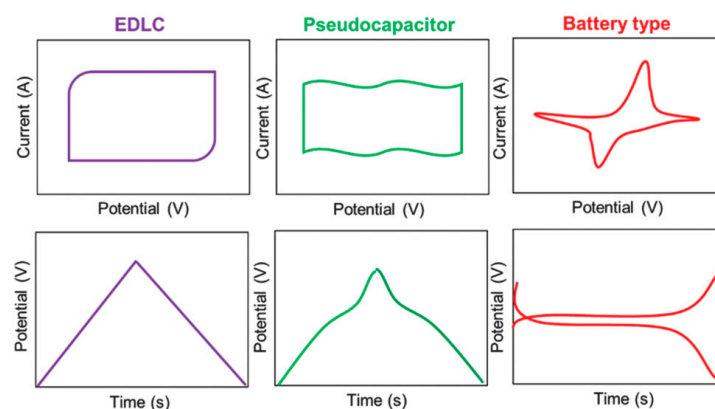


Figure 2. Demonstrative cyclic voltammetry (CV) galvanostatic charge-discharge (GCD) curves of EDLC, pseudocapacitive, and battery-type behaviours. Reprinted with permission from [40]. Copyright 2020, Royal Society of Chemistry.

3. Material Structural and Morphological Features Influencing the Electrochemical Storage Performance

A set of functional properties, including high electrical conductivity and hydrophilicity, make MXene materials promising candidates for the energy storage devices, such as

electrochemical ion batteries and supercapacitor electrodes. However, in comparison with other carbon or metal compounds, MXenes face many challenges for their practical application in the field of electrical energy storage. Complex chemical composition, terminated surface groups and interlayer space are counted as belonging to the main features that affect MXene properties, and as a result, their application performance [29,33,42,43].

Besides, the morphological features of MXene materials play a vital role in the performance of batteries and supercapacitors by significantly contributing to the electrochemical charge storage mechanism. The morphologies of 2D MXene materials can be controlled using different functional mechanisms to make them superior for charge storage. A significant increase in capacitance can occur if the water (H_2O) molecules can confine into the two-dimensional slits of MXenes stacks resulting from the etching of A layer of MAX phase. The dipolar polarization with a negative dielectric constant of these confined H_2O molecules can screen an external electric field and thus increases the EDL capacitance boosting the ion's diffusion through MXenes layers [44]. Maleski et al. investigated size-dependent physical and electrochemical properties of 2D titanium carbide ($Ti_3C_2T_x$) MXene flakes synthesized by solution-processable techniques [45]. It was observed that $Ti_3C_2T_x$ nanoscale-sized flakes with lateral sizes of $\sim 1 \mu m$ exhibited the highest specific capacitance of 290 F/g @2 mV/s and good rate performance with 200 F/g at 1000 mV/s.

Dynamic light scattering (DLS) curves (Figure 3a) represent that the 12–9 mL fraction is composed of nanoscale-sized flakes (shown in the top portion of the centrifuge tube in insert) exhibited a DLS peak of ~ 400 nm and the 6–3 mL fraction of primarily larger size flakes shown in bottom part of the centrifuge tube exhibited a DLS peak of $\sim 1.7 \mu m$. Cross-section scanning electron microscope (SEM) images (Figure 3b) displayed that for the large-flake (6–3 mL) and small-flake (12–9 mL) electrodes, respectively, due to the presence of a different concentration of $Ti_3C_2T_x$ nanoscale-sized flakes in the solution. Similar CV profiles (Figure 3c) and EIS (Figure 3d) investigation exhibited resistance differences between the two-density gradient-separated electrodes.

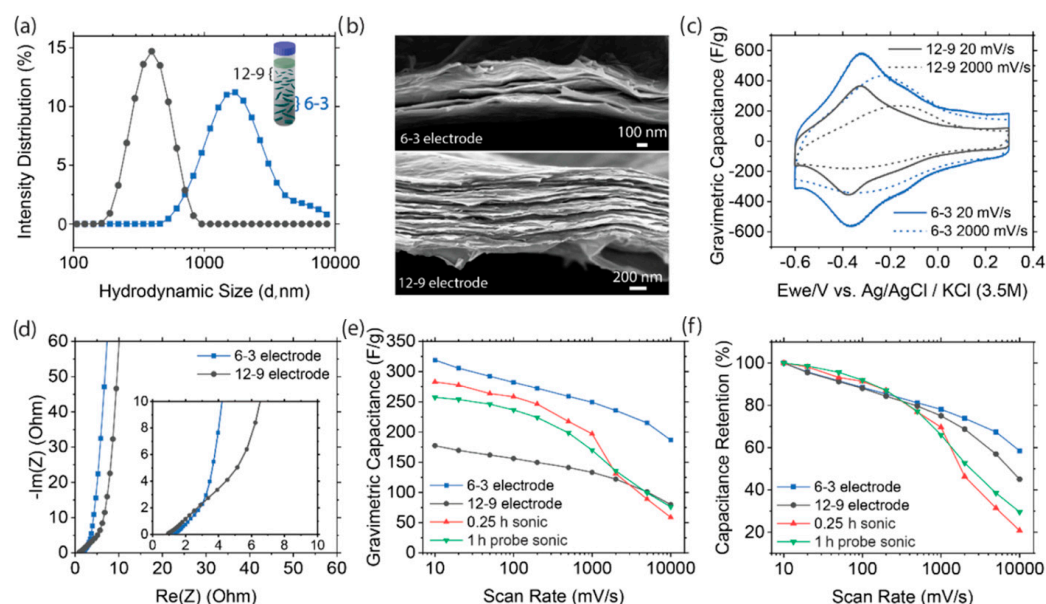


Figure 3. (a) Dynamic light scattering of the 6–3 mL fraction (blue) and the 12–9 mL fraction (black); (b) Cross-sectional SEM of the 6–3 electrode and the 12–9 electrode; (c) Cyclic voltammety curves in 3M H_2SO_4 electrolyte at different scan rates; (d) EIS curves for electrodes obtained by density gradient centrifugation with a high-frequency range in the inset; (e) Gravimetric capacitance vs scan rate; (f) capacitance retention of the BS–0.25 h sonic (red triangles), PS–1.0 h sonic (green triangles), 6–3 electrode (blue squares), and the 12–9 electrode (black circles). Reprinted with permission from [45]. Copyright 2018, American Chemical Society.

The lowest resistance of larger MXene flakes (6–3 electrode in Figure 3b) may be due to the increased electronic conductivity of the film and the thinner film increases the accessibility of the electrolyte, which leads to the increase in the diffusion of electrolyte. However, the 6–3 electrode delivered a specific capacitance of 319 F/g at 10 mV/s and 249 F/g at 1000 mV/s compared with other electrode materials (Figure 3e). Overall, $\text{Ti}_3\text{C}_2\text{T}_x$ nanoscale-sized flakes separated by density gradient with thinner electrodes exhibited better capacitance retention at high scan rates (Figure 3f). On the other hand, the core-shell type of morphology of MXene-based electrodes also showed excellent electrochemical performance with a reversible capacity of 220 mAh/g @ C/18 cycling rate over 30 cycles. These researchers also provide the information that the improvement of the energy storage capacity of MXene electrodes can be achieved by optimizing the desired morphologies of the electrode materials while tuning the oxidation process could be an effective method. There is plenty of future research scope in the formation of desired morphologies leading to increased electrochemical properties [24,46,47].

3.1. Chemical Composition

The improvement of MXenes' electrochemical performance can be achieved by optimizing and engineering their compositions. In this case, both MXenes atomic layer structure and chemical composition play an important role. For instance, MXene structures with fewer atomic layers, such as M_2X , (Figure 4) should have higher gravimetric capacities characterized by higher specific surface areas in comparison with higher order MXenes, such as M_3X_2 or M_4X_3 (Figure 4) [30]. The effect of the material's weight on its electrochemical performance was proved by Naguib et al. In their previous work, the authors demonstrated that Ti_2CT_x can be characterized by higher specific capacity in comparison to the one obtained using the same synthesis method as $\text{Ti}_3\text{C}_2\text{T}_x$ [48].

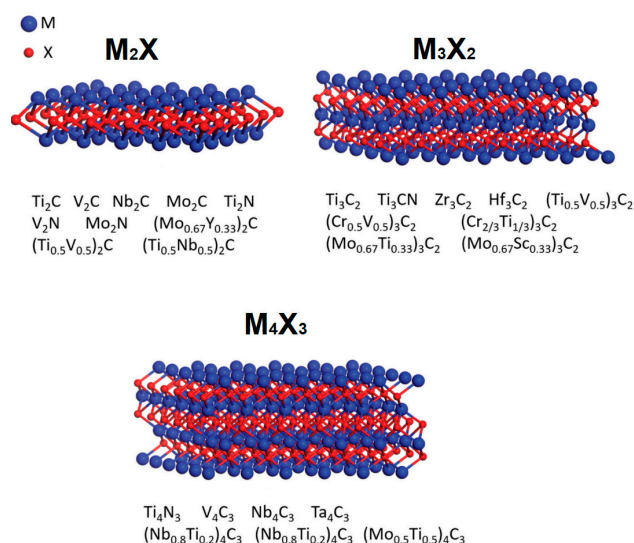


Figure 4. MXenes bare structures with an overview of all experimentally synthesized corresponding compositional samples. Reprinted with permission from [42]. Copyright © 2020, CC BY 4.0.

It was shown that complicated features of ion storage in Nb-based MXene compound lead to the higher specific capacity of Nb_2CT_x compared to Ti_2CT_x [8]. On the other hand, V-based MXenes are promising electrodes for Li-ion batteries due to their good capabilities to handle high charge-discharge rates and the highest Li capacity values among all transition metals [36,49]. For instance, Naguib et al. [30] have demonstrated great perspectives of the layered Nb_2CT_x and V_2CT_x powders (see Figure 5a,b), fabricated via a selective etching approach, as electrode materials in Li-ion batteries for high-power applications. According to the cyclic voltammetry (CV) investigations (see Figure 5c,d), the electrochemical performance and voltage profile of the MXene materials depends significantly on their chemistry. Thus, for the Nb_2CT_x no significant lithiation/delithiation

capacity has been observed at the voltages above 2.5 V, while CV curves of V_2CT_x exhibited larger capacity at voltages close to the 3 V. On the other hand, both Nb_2CT_x and V_2CT_x showed excellent capability (110 mAh/g for Nb_2CT_x and 125 mAh/g for V_2CT_x after 150 cycles) and good reversible capacity (99.6% for Nb_2CT_x and 98% for V_2CT_x) at high cycling rate of 10C (see Figure 5e). Authors have also demonstrated that in addition to the MXene chemistry, the great effect of the powder processing. Thus, V_2CT_x , produced from the milled V_2AlC MAX phase, showed significant enhancement in Li uptake (>30%) compared to the MXene material produced from the unmilled MAX phase. The improvement in Li uptaking process authors explained by the decreased particle sizes and, as a result, faster Li diffusion between layers.

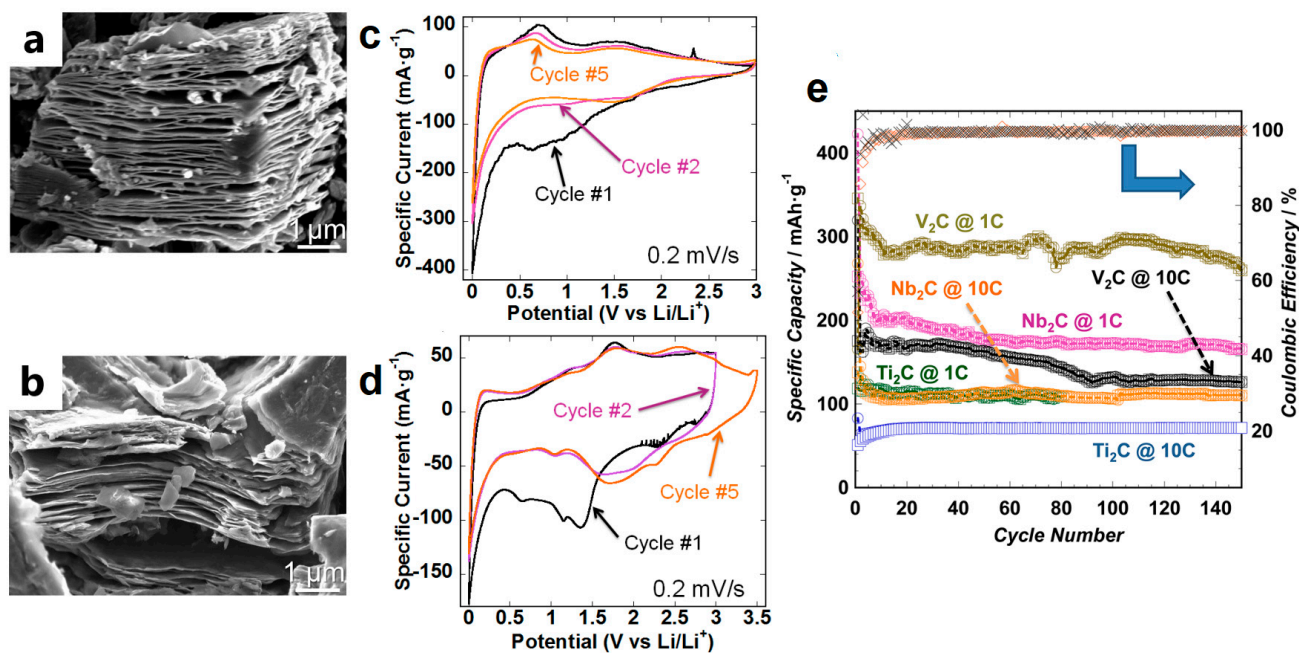


Figure 5. (a) SEM images of Nb_2CT_x powder; (b) SEM images of V_2CT_x powder; (c) Cyclic voltammograms for Nb_2CT_x ; (d) Cyclic voltammograms for V_2CT_x ; (e) Specific capacities vs cycle number at different rates for Nb_2CT_x and V_2CT_x -based electrodes. Reprinted with permission from [30]. Copyright © 2013, American Chemical Society.

Besides variation in chemical composition, the capacity improvement of the MXene-based electrodes can be achieved by the formation of MXene hybrids in a combination of other electrochemical materials [28]. A good example is given in the work of Luo et al. [50] who applied a facile liquid-phase immersion process based on ion-exchange interactions and electrostatic interaction for the synthesis of Sn^{4+} -decorated Ti_3C_2 nanocomposites (see Figure 6a–c). Its characterization yielded improved volumetric capacity, high Coulombic efficiency and excellent cycling stability. Cyclic voltammetry investigations showed good reversibility of PVP- $Sn(IV)@Ti_3C_2$ composites during the electrochemical performance. CV curves, recorded at a scan rate of 0.1 mV/s, demonstrated the presence of four reduction peaks, corresponding to solid electrolyte interphase (SEI) formation, electrolyte decomposition and $Sn(IV)$ nanocomplex reduction (peaks around 1.5 and 1.15 V); trapping of Li-ion between MXene sheets (peak around 0.75 V); Li intercalation and Li_xSn formation (dominant peak between 0.5 and 0 V). From another side, three oxidation peaks have been observed during the anode sweep, which may be referred to: Li^+ delithiation from the Li_xSn alloy (peak around 0.5 V); Li^+ extraction from the MXene matrix (peaks around 1.5 and 2 V) (see Figure 6d). Based on CV results, authors have assumed that electrochemical interaction between Li and PVP- $Sn(IV)@Ti_3C_2$ takes place in two stages: (1) electrochemical reaction of Li^+ with $Sn(IV)$ complex; (2) electrochemical reaction of Li^+ with Ti_3C_2 MXene matrix. Moreover, they have demonstrated that PVP- $Sn(IV)@Ti_3C_2$

composites fabricated via a facile polyvinylpyrrolidone (PVP)-assisted liquid-phase immersion process (see Figure 6e) provide improved charge transfer performance (see Figure 6f) relying on excellent electron conductivity.

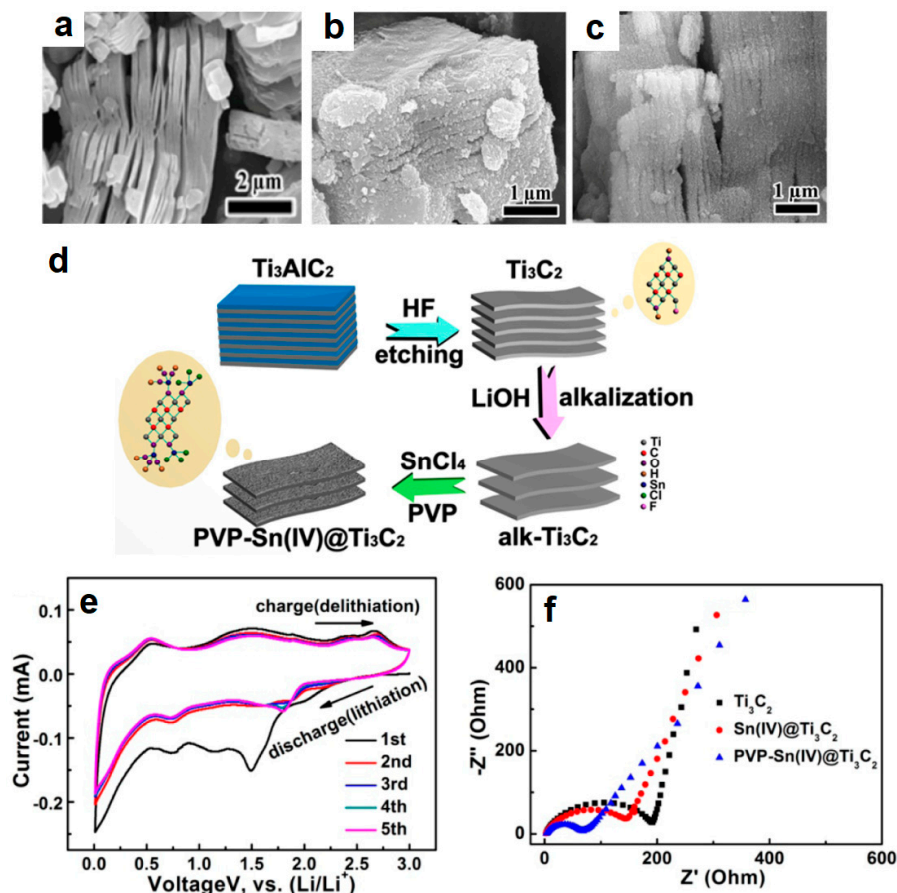


Figure 6. (a) SEM image of Ti₃C₂ nanosheets; (b) SEM image of Sn(IV)@Ti₃C₂ composites; (c) SEM image of PVP-Sn(IV)@Ti₃C₂ nanocomposites; (d) Schematic illustration of the polyvinylpyrrolidone (PVP)-assisted liquid-phase immersion process to produce PVP-Sn(IV)@Ti₃C₂ nanocomposites; (e) CV curves of PVP-Sn(IV)@Ti₃C₂ nanocomposites; (f) Nyquist plots at 100 kHz to 10 mHz of the Ti₃C₂, Sn(IV)@Ti₃C₂, and PVP-Sn(IV)@Ti₃C₂ electrodes. Reprinted with permission from [50]. Copyright © 2016, American Chemical Society.

Li-ion batteries having electrodes consisting of MXene/Metal oxides composite exhibited high power and energy densities, as well as high rate performance [28]. Similar observations were made by Ahmed et al. [51] who have grown SnO₂ on two-dimensional Ti₃C₂ sheets resulting in high Li-ion capacity, as attributed due to both structural and mechanical strengths of SnO₂ and conductivity of MXenes. It has been reported that obtained composites provide excellent electrochemical performance at the Li-ion battery anodes, besides, the layered structure of MXenes prevents the disadvantageous volume changes that may occur during the lithiation and delithiation via SnO₂.

In their study, Zhang et al. demonstrated good electrochemical characteristics of Nb₂O₅@Nb₄C₃T_x composites, synthesized using a one-step high-temperature oxidation process in flowing CO₂. The authors have attributed the improved performance of the obtained composites is due to the synergetic effect between the metal oxide and MXene platform, i.e., Nb₂O₅ nanoparticles provide fast rate response and high capacity while Nb₄C₃T_x layers assure high conductivity [52].

Another strategy is the decoration of MXene sheets with metal nanoparticles which also leads to the improved performance of the MXenes-based anodes of the Li-ion batteries. A striking example is given by the formation of MXene/Ag composites that resulted in high

charge-discharge rates with extraordinary stability and long cycle lifetimes. In their work, Zou et al. [53] investigated the electrochemical performance of Ti_3C_2 structures, decorated with Ag nanoparticles (Figure 7a,b). The results of CV investigations indicated that in both pure MXene and MXene/Ag nanocomposites charge storage mechanism is due to the Li^+ intercalation rather than a conversion reaction (Figure 7c,d). On other hand, the additional peak was detected for the MXene/Ag nanocomposites at around 0.37 V, which may be referred to as the Li-ions extraction from the MXene/Ag electrodes (Figure 7d). The presence of the additional peak authors has been explained by the formation of the transition-state Ti during the reduction process with its following transformation to the stable Ti after cycling. The synthesized $\text{Ti}_3\text{C}_2/\text{Ag}$ composites have demonstrated high reversible capacities (310 mAh/g@1C; 260 mAh/g@10C; 150 mAh/g@50C) and stable performance over 5000 cycles (Figure 7e), which may be as well explained by the Ti (II) to Ti (III) during the cycling process.

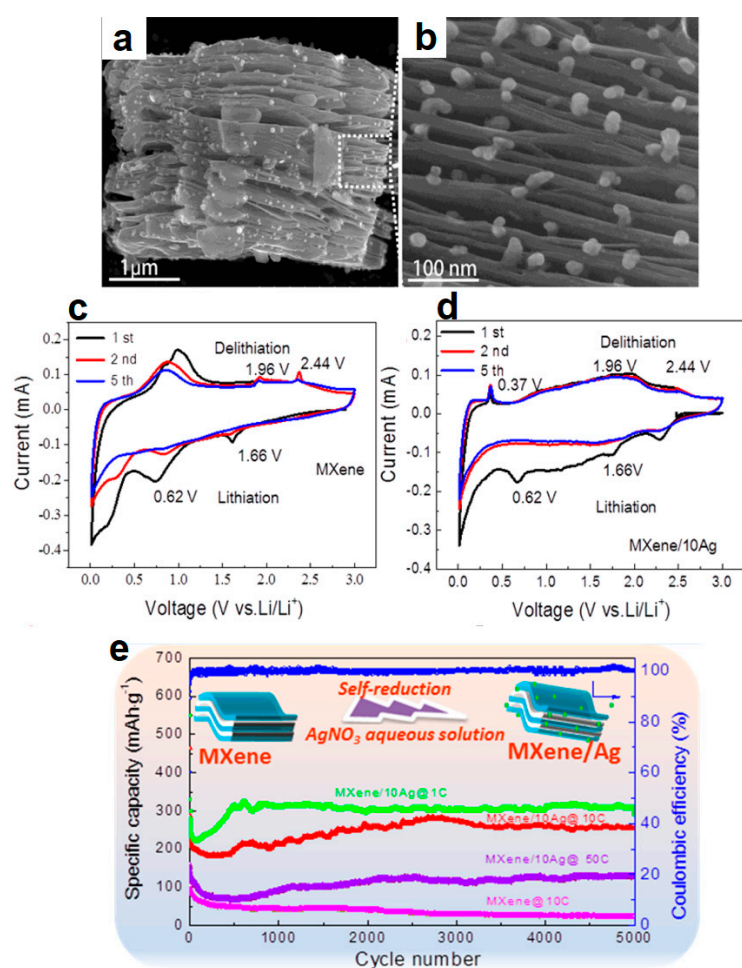


Figure 7. (a,b) SEM images of $\text{Ti}_3\text{AlC}_2/\text{Ag}$ composites; (c,d) Cyclic voltammograms of Ti_3C_2 and of $\text{Ti}_3\text{C}_2/\text{Ag}$ composites; (e) Specific capacity vs cycle number and coulombic efficiency of $\text{Ti}_3\text{AlC}_2/\text{Ag}$ composite. Reprinted with permission from [53]. Copyright © 2016, American Chemical Society.

Silicon (Si) is known as one of the most promising negative electrodes for LIBs owing to their high theoretical specific capacity, suitable Li-intercalation/deintercalation potential range and abundant resources. However, poor cycling and rate performances due to the huge volume change during lithiation/delithiation limits their practical applications in LIBs. Various Si-based composite structures are studied to improve electrode stability and electrical conductivity without compromising the structural integrity of negative electrode materials. From the materials perspective, 2D MXenes have increasingly attractive as Si-incorporated negative electrode processing, such as $\text{Si}/\text{Ti}_3\text{C}_2\text{T}_x$ because of their several

advantages such as silicon nanoparticles (SiNPs) can easily incorporate into their layered structures and form various composites, increase active charge carrier conduction in Si-based electrodes etc. which can significantly improve electrode performance in LIBs. The layered structure of MXene compounds provides room for the volume expansion and shrinkage of Silicon. Moreover, MXenes surface terminated groups show a tendency to bond with silicon, which decreases the probability of the reactions with electrolytes [54]. Li et al. demonstrated that the combination of MXene nanosheets with Si nanoparticles allows rapid electron and ion transfer, resulting in an anode material's capacity as high as 1422 mAh/g, excellent cycle stability and good rate performance [55].

Using various synthesis processes including mechanical or ball milling mixing, magnesiothermic reduction, wet processing, vacuum-assisted filtration, spray drying, freeze-drying etc. Si/MXenes can be synthesized. Variation of the Si/MXenes interface can efficiently enhance the interactions between silicon and MXene materials as well as regulate the surface reaction of the SiNPs. It has been observed that the Si/MXene-based electrodes showed great potential for future energy storage applications. However, the surface functional groups such as -O, -OH, -F etc. in MXenes sometimes decrease the reaction possibility with electrolytes due to the tendency to bond with silicon, which needs to be overcome. Suitable surface functionalization of oppositely charged SiNPs and MXenes could be one of the effective approaches due to the presence of their surface terminal groups [54].

On the other hand, Sobyra et al. investigated the dynamical structural response of the electrode materials based on $Ti_3C_2T_x$ MXenes during the electrochemical intercalation of ions. The time-resolved operando X-ray reflectivity was measured during cyclic voltammetry (CV) investigations. They observed that the dynamic structure of MXenes plays a significant role in their functionality in high-power energy storage devices. Usually, the MXene electrodes showed two different charging regimes including both capacitive and non-capacitive (redox) characteristics corresponding to kinetically limited lithium intercalation and layer contraction. Slow and fast lattice contraction regimes with respect to the applied potential were also observed as related to the capacitive and redox features, respectively, during electrochemical ion intercalation. These studies revealed that the slow spacing contraction MXene-layer is because of the limited diffusion control process and the following rapid contraction related to the redox reaction without diffusion limitations [56].

Xia et al. also reported the thickness-independent capacitance of vertically aligned liquid crystalline 2D titanium carbide ($Ti_3C_2T_x$) MXenes synthesized by mechanical shearing of a discotic lamellar liquid crystal (LC) phase of $Ti_3C_2T_x$ for large-scale electrochemical energy storage (EES) applications. These $Ti_3C_2T_x$ MXenes films exhibited excellent rate capability and nearly thickness-independent performance up to 200 μm . This thickness-independent capacitive performance is making them highly attractive for next-generation energy storage applications [57].

Due to their unique properties, MXene-based materials can also be used in other metal-ion battery types, including Na-ion batteries [58,59], K-ion batteries [60], Al-ion batteries [61], Mg-ion batteries [62], LiS [63] and NaS batteries [64]. Compared to the Li-ion batteries, these alternative metal-ion batteries can provide relatively high power and energy density, large storage capacity, operational safety and environmentally friendly nature by the employment of abundant and low-cost materials [9,65]. Similarly, to Li-ion batteries, the choice of electrode materials is crucial for ion transport and overall electrochemical performance. From this point of view, MXene-based compounds are considered as perspective materials in realizing high-performance non-Li batteries, owning high conductivity, large surface area, excellent flexibility, strong polar surface and tendency to accommodate a variety of cations [9,34]. However, to achieve the improved specific capacity of non-Li batteries the modification of MXene structures is essential [35]. For instance, in their research Bao et al. [64] have demonstrated that MXenes doping with sulfur ions leads to increased capacity and longer cyclability of NaS batteries. On the other hand, the incorporation of Sb into the $Ti_3C_2T_x$ matrix improves the charge transfer kinetics and enhances the storage capability of K-ion batteries [60].

Table 1 summarizes the performance of MXenes and MXene-based composites in different battery types.

Table 1. Performance of MXene-based structures in batteries.

Electrode Material	Synthesis Approach	Mass Loading, mg/cm ²	Electrolyte	Capacity	Ref.
Li-ion batteries					
Nb ₂ AlC V ₂ AlC	HF-etching	N/A *	1M LiPF ₆ / EC, DEC	170 mAh/g@1C 110 mAh/g@1C	[30]
PVP-Sn(IV)@Ti ₃ C ₂	Liquid-phase immersion	N/A *	1M LiPF ₆ / EC, DEC	635 mAh/g	[50]
HfO ₂ @Ti ₃ C ₂ /SnO ₂	Atomic layer deposition	N/A *	1M LiPF ₆ / EC, DMC	843 mAh/g	[51]
Nb ₂ O ₅ @Nb ₄ C ₃ T _x	One-step oxidation	2.65	1M LiClO ₄ / EC, DMC	208 mAh/g@0.25C	[52]
Ti ₃ AlC ₂ /Ag	HF-etching/ AgNO ₃ reduction	N/A *	1M LiPF ₆ / EC, DMC	310 mAh/g@1C 260 mAh/g@10C	[53]
Hf ₃ C ₂ T _z	HF-etching	0.5–0.7	1M LiPF ₆ / EC, DMC	145 mAh/g	[58]
Ti ₃ C ₂	Delamination	3.0	1M LiPF ₆ / EC, DEC	410 mAh/g@1C	[66]
Ti ₃ C ₂	DFT computations	N/A *	N/A *	320 mAh/g@	[67]
Ti ₃ C ₂ T _x /CNT	HF-etching	0.6–1.0	1M LiPF ₆ / EC, DEC	1250 mAh/g@0.1C	[68]
Ti ₃ C ₂ /TiO ₂ Ti ₃ C ₂ /SnO ₂	HF-etching/ Self-assembling	1.0–1.1	1M LiPF ₆ / EC, DEC	209 mAh/g@0.5 A/g 530 mA·h·g ⁻¹ /1 A/g	[69]
Ti ₃ C ₂ /Fe ₃ O ₄	Sonication	1.5–2.0	1M LiPF ₆ / EC, DMC, EMC	747 mAh/g@1C	[70]
Ti ₃ C ₂ /CoO	Hydrothermal	N/A *	1M LiPF ₆ / EC, DMC	324 mAh/g@0.1 A/g	[71]
Ti ₂ CT _x /Si	Covalently anchoring silicon nanospheres	N/A *	1M LiPF ₆ / EC, DEC	1670 mAh/g@1 A/g	[72]
Na-ion batteries					
Hf ₃ C ₂ T _z	HF-etching	0.5–0.7	1M LiPF ₆ / EC, DMC	47 mAh/g	[58]
Ti ₂ CT _x	HF-etching	1.0	1M NaPF ₆ / EC, DEC	40 mAh/g@1C	[59]
S-ion batteries					
S/Ti ₂ C	HF-etching/ melt diffusion	1.0	1M LiTFSI/DME, DOL/LiNO ₃	1200 mAh/g@5C	[73]
NaS batteries					
Ti ₃ C ₂ T _x /S	LiF/HCl etching	4.5	2M NaFSI/ EC, DEC	577 mAh/g@2C	[64]
Al-ion batteries					
Ti ₃ C ₂ T _x /Co ₉ S ₈	LiF/HCl etching/ thermal-induced carbonization/sulfidation	0.8–1.0	IL-electrolyte	288 mAh/g@1 A/g	[61]
K-ion batteries					
Ti ₃ C ₂ T _x /Sb	LiF/HCl etching/ hydrothermal	1.0	1M KFSI/ EC, PC	314 mAh/g@1 A/g	[60]
Ti ₃ C ₂ T _x /MoSe ₂	LiF/HCl etching/ hydrothermal	1.0	1M KFSI/ EC, DEC	183 mAh/g@10 A/g	[74]

* The data is not provided.

MXenes have also shown promising pseudocapacitive performance in supercapacitors owing to their unique structure, rapid ion diffusion and fast electron transport capability [75,76]. Table 2 represents some recent works on MXene-based electrodes in supercapacitors and their electrochemical performance.

Moreover, recent works have exhibited that the combination of 2D MXenes with transition metal sulfides (TMS) or transition bimetal sulfides producing heterostructure nanocomposite can enhance the specific capacitance value, long cycle stability as well as increase the rate-capability of pristine MXene-based electrode materials [77]. These heterostructured composite materials at electrodes increase the number of active sites within the highly exposed 2D layers for ion intercalation creating synergistic effects for possible physical/chemical adsorption as well as chemical reaction processes, etc. Ruan et al. [78] have employed ZIF-67 flake as a precursor for transforming CoNi_2S_4 dendrites in MXene suspension by a controlled synthesis to obtain Ti_3C_2 MXene-wrapped CoNi_2S_4 nanotrees grown on nickel foam. These Ti_3C_2 MXene-wrapped CoNi_2S_4 nanotrees offered a good rate performance of 70.2% exhibiting a ten-fold increase in current density with a high specific capacity of 933 C/g @ 1 A/g counting on the unique dendritic morphology providing a high number of electro-active sites. In this research work, it was also shown that the wrapped conductive MXene can facilitate charge transfer yielding higher supercapacitor device performance. Xu J. and co-workers developed ultrathin Ti_3C_2 MXenes doped with NiMoS_4 nanoparticles by a hydrothermal method with the assistance of dopamine (DA) and applied these to supercapacitor electrodes. They found that the dopamine was adsorbed by the Ti_3C_2 surface forming a negatively charged layer and enriching the metal ions. This unique heterostructure Ti_3C_2 -DA- NiMoS_4 material increased the exposed NiMoS_4 active sites and solved the problem of specific capacitance loss due to volume changes [79]. Although, MXenes enhance the electrochemical energy storage performance of the MXene-based composite electrodes by boosting electroactive sites across the 2D architecture and their high electrical conductivity. On the other hand, the low-energy density of MXene-based aqueous hybrid supercapacitors limits practical device implementation. In order to improve the specific energy density, Javed et al. have produced nickel-cobalt-sulfide (NCS) nanoflowers embedded in exfoliated $\text{Ti}_3\text{C}_2\text{T}_x$ MXene layers (HS-NCS@MXene) yielding heterostructured (HS) composites and investigated for supercapacitive performance [80]. This HS-NCS@MXene displayed promising pseudocapacitive performance on measurements with a three-electrode system yielding capacitance of 2637 F/g at 2.5 A/g with 96% capacity retention of the initial value over 10,000 cycles. These studies prove that the rational design of transition bimetal sulfides in MXene layers is extremely beneficial as electrode materials for SCs. The recent development of various MXene-based electrodes, their synthesis methods and their electrochemical performance as supercapacitor applications have been summarized in Table 2. It can be observed from Table 2 that MXene-based electrodes not only provide a promising electrochemical performance through high specific capacitance, high energy density, and power density in a high potential window relative to the electrolyte, but they also exhibit excellent capacity retention over a long cycle, which can make them promising for future supercapacitor device applications.

Table 2. Performance of MXene-based electrodes in supercapacitors.

Electrode Material	Synthesis Approach	Electrolyte	Electrochemical Performance	Capacity Retention (%)	Ref.
Asymmetric supercapacitors					
HS-NCS/ $\text{Ti}_3\text{C}_2\text{T}_x$	HF-etching/ Hydrothermal	2M KOH	1.6 V 226 F/g @ 1.5 A/g 80 Wh/kg 1196 W/kg	92% for 20,000 cycles	[80]
$\text{Ti}_3\text{C}_2\text{T}_x$	Etching route	1.5M ZnSO_4	1.2V 214 mF/cm ² @ 5mV/s 42.8 $\mu\text{Wh}/\text{cm}^2$ 0.64 mW/cm ²	83.58% after 5000 cycles	[81]

Table 2. Cont.

Electrode Material	Synthesis Approach	Electrolyte	Electrochemical Performance	Capacity Retention (%)	Ref.
Ti ₃ C ₂ T _x	Layer-by-layer assembly	ACN-PC-PMMA-LiCF ₃ SO ₃ gel electrolyte	1.2V 40.8 mF/cm ² 8.2 μWh/cm ² 630.1 μW/cm ²	90% after 200 bending cycles	[82]
V ₂ NT _x	LiF–HCl-etching	3.5M KOH	1.8 V 25.3 F/g @ 1.85 mA/cm ²	96% after 10,000 cycles	[83]
Symmetric supercapacitors					
Nb ₂ C/Ti ₃ C ₂	Chemical etching	1M PVA/H ₂ SO ₄ gel electrolyte	1.3 V 53 F/g @ 0.3 A/g 12.5 Wh/kg 1535 W/kg	98% for 50,000 cycles	[84]
Mo _{1.33} CT _z	HF-etching	19.5M LiCl	1.8 V 140 F/cm ² @ 0.5mA/cm ² >41.3 mWh/cm ³ 165.2 mW/cm ³	82.1% for 50,000 cycles	[85]
Ti ₃ C ₂ /BCN	Etching/ pyrolysis	1M PVA/H ₂ SO ₄ gel electrolyte	1.6V 245 F/g ¹ @ 1 A/g 22 Wh/kg 8004 W/kg	100% after 100,000 cycles	[86]
Ti ₃ C ₂ T _x 3D Aerogels	Bioinspired freezing method	PVA/H ₂ SO ₄ gel electrolyte	0.6V 230 mF/cm ² @5 mV/s 38.5 μWh/cm ² 1375 μW/cm ²	86.7% after 4000 cycles	[87]
Ti ₃ C ₂ /Copper/Cobalt Hybrids	Lewis Acidic Molten Salts Etching	1.0M H ₂ SO ₄	1.6 V 290.5 mF/cm ² @1 mA/cm ² 103.3 mWh/cm ² 0.8 mW/cm ²	89% after 10,000 cycles	[88]
Ti ₃ C ₂ T _x film	in situ etching	H ₂ SO ₄	345 F/g @ 2 mV/s 14.1 Wh/L 135.2 W/L	88.5% after 5000 cycles	[89]
Micro-supercapacitors					
PANI@rGO/Mxenes	Solution method	PVA-PAA-NHS hydrogel	2V 45.62 F/g ¹ 1.585 Wh/kg 25.48 W/kg	84% after 10,000 cycles	[90]
MXene/BC@PPy	Vacuum-filtration	2M Zn(CF ₃ SO ₃) ₂ -0.1M MnSO ₄ /PAM hydrogel	1.9V 290 mF/cm ² 145.4 μWh/cm ² 3.78 mW/cm ²	95.8% after 25,000 cycles	[91]
Ti ₃ C ₂ T _x	Multiscale structural engineering	PVA/H ₂ SO ₄ Gel Electrolyte	0.6V 2.0 F/cm ² 0.1 mWh/cm ² 0.38 mW/cm ²	90% after 10,000 cycles	[92]
Three-electrode cell					
Ti ₃ C ₂ T _x	HF-etching	1M EMIMTFSI/ACN	3,2V 185 F g ⁻¹ @ 0.2 A/g 370 Wh/kg 46 kW/kg	97% after 10,000 cycles	[25]
Ti ₃ C ₂ T _x /graphene/Ni	Supernatant during etching and washing processes	aqueous acidic	1V 254 F g ⁻¹ @ 1 A/g 35.28 Wh/kg 18.144 kW/kg	90% after 5000 cycles	[93]
Ti ₃ C ₂ T _x	Electrospray Deposition Technique	1M H ₂ SO ₄	0.8V 400 F/g	90% after 10,000 cycles	[94]
CoF/MXene	HF-etching/ ultrasonication	0.1M KOH	0.5V 1268.75 F/g @ 1 A/g	97% after 5000 cycles	[95]
V ₂ C	HF-free etching process	1M Na ₂ SO ₄	0.6V 164 F/g @ 2 mV/s	90% after 10,000 cycles	[96]

Symmetric supercapacitors (SSCs) have typically no charge imbalance issues due to their voltage window being equal to the voltages of both positive and negative electrodes. Therefore, MXene-based SSCs with wide voltage windows can deliver high energy densities. Applying as a typical negative electrode material, MXene-based electrodes usually exhibit lower potential than +0.3 V vs. Ag/AgCl and over this potential, oxidation occurs for MXenes resulting in deterioration of structural stability. Gogotsi et al. observed that $Ti_3C_2T_z$ MXene electrodes could lead to higher potential (>+0.6 V vs. AgCl or +0.8 V vs. Ag wire) in highly concentrated LiCl electrolytes which also offers an opportunity to break the limitation of positive potential for MXene-based SSCs [97]. In recent work, Zheng et al. developed MXene-based SSC electrodes by applying different etching processes for surface terminations varying from -F, -OH, -O, -Cl which is indicated with T_z . The electrochemical performance investigations of this electrode were carried out by using a highly concentrated LiCl electrolyte. The surface-terminated $Mo_{1.33}CT_z$ MXene-based SSCs provided a higher potential of 1.4 V and delivered a maximum energy density of >38.2 mWh/cm³ at a power density of 196.6 mW/cm³ with good recyclability [85].

Specifically, MXenes with their unique layered structures and excellent conductivities deliver high specific capacitance as supercapacitor electrodes in commercial aqueous electrolytes. Lukatskaya et al. synthesized macroporous $Ti_3C_2T_x$ MXene films delivering up to 210 F/g at a scan rate of 10 V/s in an H_2SO_4 aqueous electrolyte. They also reported that MXene hydrogels can store a volumetric capacitance of ≈ 1500 F/cm [98]. Although aqueous electrolytes can offer high specific capacitance for supercapacitors, however lower potential range (up to 1.2 V is to face due to water splitting reaction) limits the attainment of high energy density. Furthermore, high oxidation of MXene electrodes under higher anodic potentials (>1.2V) in aqueous electrolytes bounds their use as cathodes in ASC devices. Thus, to improve the energy density of MXene-based electrodes in supercapacitors, the increase of the operating voltage window could be an effective alternative approach [25].

A practical application of MXenes electrode-based supercapacitors was given by Liu Y. and co-workers who fabricated PANI@rGO/MXenes as electrodes for lightweight, thin, stretchable, and wet-adhesive all-hydrogel micro-supercapacitor (MSC) and for the first time, implanted onto the heart of living mice (Figure 8). This all-hydrogel micro-supercapacitor delivered high areal capacitance (45.62 F/g) and energy density (333 μ Wh/cm², 4.68 Wh/kg). The study of its electrochemical performance and biocompatibility of the all-hydrogel MSC was carried out using two models (in vitro cell tests and in vivo mice). The immunohistochemical analysis and the immunofluorescent staining of biomarkers of mice tissues were investigated after 14 days of implantation. The results have revealed that biocompatible MSC implantation had negligible effects in living mice. This research suggests promising SC application for bioelectronics and shed light on future bio-integrated electronic energy storage systems [90].

Even though remarkable progress is achieved in the field of MSCs, the lower specific capacitance of the carbon-based materials (AC, CNT, graphene etc.) on the EDLC storage mechanism and a small electrode thickness have strictly restricted the energy density for such MSCs. Therefore, the development and fabrication of battery-type MSC electrode materials could be a promising alternative for overcoming the familiar challenge of a capacity mismatch for MSCs toward their commercial application. On this aspect, 2D MXenes with a multi-layered structure and higher metallic conductivity can enhance the charge storage capability in a short time via significant intercalation of ions between the multilayers of MXene-based electrodes providing an ideal candidate for MSC electrode material applications [91,99].

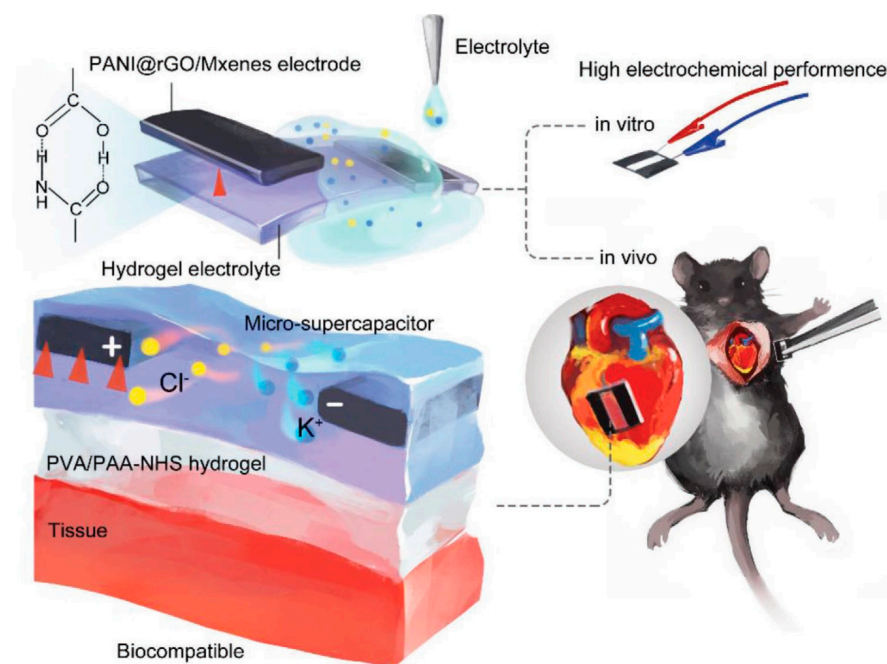


Figure 8. Schematic illustration of the fabrication process and implantation of micro-supercapacitor onto the heart of living mice. Reprinted with permission from [90]. Copyright 2021, Wiley Online Library.

3.2. Surface Terminations

As indicated above, the chemical composition has a crucial role in the MXenes' electronic properties and their electrochemical performance. However, one of these properties, the conductivity of MXene-based materials can be controlled by tailoring their surface chemistry. Thus, MXenes' surface termination groups (-OH, -O, -F), introduced during the synthesis, affect strongly Fermi level density of states, electronic conductivity and thereby MXenes' functional properties [28].

To date, several density functional studies (DFT) have been performed which investigate the structural and electronic properties of MXene compositions with different surface terminations. In early works, it was predicted that surface functionalization of the most studied MXene compound $Ti_3C_2T_x$ reduces the Fermi level density of states, resulting in a conductivity decrease [67,100,101]. Hart et al. demonstrated in their work that the loss of -OH groups cause the decrease of resistance of $Ti_3C_2T_x$, while the removal of -F terminations leads to conductivity improvement [29]. Garg et al., reported that $Ti_3C_2T_x$ with -OH and -F terminals on the surface exhibits a higher diffusion barrier compared to the low energy barrier and easy Li-ion migration in the case of bare $Ti_3C_2T_x$ [9].

The structural optimizations and the calculation of the electronic structure performed with the OH-, F- and O-terminated MXenes led to the conclusion that F- and O-terminated MXene materials are characterized by the high energy of near-free electron states [102]. Xie et al. have demonstrated that MXenes with O-terminations are able to adsorb two Li atomic layers, resulting in the highest values of the theoretical Li-ion storage capacities [49].

3.3. Lamellar Stacking

The morphological and structural features of MXenes highly affect the transport of solvent molecules and the cations' intercalations/deintercalations during charge and discharge. From this perspective, interlayer space between MXenes nanosheets, providing the natural channels for the ions' transport, plays an important role in the MXenes' electrochemical performance [33]. The fact is that the stacking of 2D MXene sheets hinders the ions' transport, resulting in low electrochemical performance and limited energy storage capacity [103]. Alternatively, MXene materials with large interlayer spacing stand out as

promising materials for ion batteries and supercapacitors due to their high conductivity. The intercalated and non-intercalated MXene sheets are characterized by measuring the electrical resistivity yielding that the resistivity values of all intercalated MXenes were higher compared to the non-intercalated ones. This is attributed to their higher c-lattice parameter (c-LP) after intercalation. The relative expansion was correlated with the number of MXene atomic layers. Thus, MXenes with five atomic layers (M_3X_2) led to an increase by an order of magnitude in the resistivity, while three atomic-layered MXene (M_2C) compounds demonstrate a resistivity increase by two orders. As a result, delaminated MXene structures exhibit four times higher specific capacity than as-synthesized MXenes [66].

Several approaches have been proposed to prevent stacking, including natural sedimentation methods for MXene production, constructing MXene-based 3D structures, and the formation of MXene hybrid structures with other electrode materials. Moreover, prevention of layer-stacking can be possible through the formation of MXene-based 3D structures and by hybrid composites that can improve ion diffusion via the formed ion channels [33]. Wang et al. have demonstrated that self-supporting electrode film made of 3D porous MXene nanosheets/bacterial cellulose network provides rapid ion transfer, effective ion diffusion and high deformation resistance and mechanical strength. As a result, the obtained MXene/bacterial cellulose structures exhibited an ultrahigh capacitance performance of 416 F/g, 2084 mF/cm² [104].

The electrochemical performance of MXene structures can be significantly improved by combining them with other highly conductive electrode materials. For instance, the combination of MXene sheets with graphene oxide powder via filtration/spark approach at the sodium-metal batteries leads to the formation of electrode material with excellent electrochemical performance in terms of stable long-term cycling and high-capacity retention (88.3% after 280 cycles) [105].

In turn, carbon nanotubes (CNT) act as spacers between MXene nanosheets, resulting in composites with enhanced electrolyte accessibility, consequently at higher capacity values (1250 mAh/g at 0.1C; 330 mAh/g at 10C), better rate performance and excellent cycling stability of Li-ion storage devices in comparison to the pure $Ti_3C_2T_x$ MXenes sheets [68]. Similarly, Lin et al. achieved significantly improved reversible capacity, excellent rate capability and superior long-term stability using the $Ti_3C_2T_x$ /CNT composites compared to the pure $Ti_3C_2T_x$ particles [106]. Liu et al. have demonstrated that usage of TiO_2 nanorods and SnO_2 nanowires as spacers between Ti_3C_2 layers avoids the restacking of the MXene sheets, resulting in the extraordinary electrochemical properties provided by the short diffusion pathways and formation of the extra active sites [69].

4. Effect of Electrolytes on MXene-Based Supercapacitor Mechanism

To date, most of the research has focused on developing a variety of high-performance MXene-based electrode materials and fewer efforts have been devoted to investigating the effect of different electrolytes on MXene-based supercapacitors. The appropriate choice of electrolyte is very important and plays an important role in improving the supercapacitive performances of specific capacitance, energy density, power density and long-cycle durability [107]. A limited potential window of aqueous electrolytes (up to 1.2 V) restricts their practical SC device applications. On the contrary, organic electrolytes can offer higher potential up to 4 V which is beneficial for increasing higher energy density, but the high resistance and high-water content of the organic electrolytes limit the power density and practical working voltage of the SC device [108]. Among different types of electrolytes, it has been observed that room-temperature ionic liquids (RTILs) proved themselves as a promising alternative due to their high stability, low flammability and wide potential (up to 4.0 V) ability. However, RTILs as electrolytes for SC offer lower practical capacitance compared with aqueous and organic electrolytes because of their larger cation sizes such as these of 1-ethyl-3-methylimidazolium (EMIM+), 1-butyl-3-methylimidazolium (BMIM+), 1-hexyl-3-methylimidazolium (FIMIM+), and 1-octyl-3-methylimidazolium (OMIM+) than the commonly used cations (e.g., H⁺, Li⁺, Na⁺, and K⁺) of aqueous electrolytes. The acces-

sibility and fast transport of large-size RTIL-electrolyte cations are limited by the lower interlayer spacing (d-spacing) of electrode materials leading to lower capacitance values [25]. Simon et al. reported the supercapacitor application in 1-Ethyl-3-methylimidazolium bis(trifluoromethylsulfonyl) imide (EMI-TFSI) IL electrolyte of the $Ti_3C_2T_x$ MXene ionogel film, synthesized via vacuum filtration approach (Figure 9). They observed that due to the structure disordering of the $Ti_3C_2T_x$ hydrogel film and generated available stable spacing during the vacuum drying, the surface of $Ti_3C_2T_x$ MXene ionogel film became accessible to a larger number of EMI⁺ and TFSI⁻ ions. This $Ti_3C_2T_x$ hydrogel offered capacitance values of 70 F/g in a voltage window of 3 V in EMI-TFSI [109].

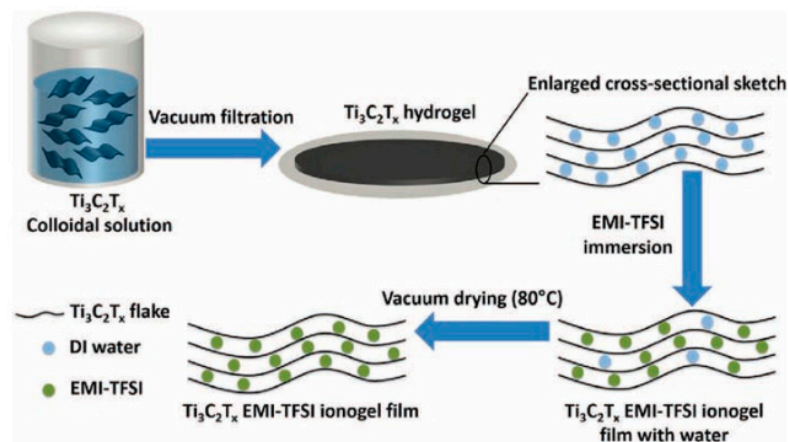


Figure 9. Schematic of the synthesis process of $Ti_3C_2T_x$ EMI-TFSI ionogel film. Reprinted with permission from [109]. Copyright 2016, Elsevier.

M. Naguib and co-workers reported that the specific capacitance and rate capability for MXene-based electrodes of supercapacitors are not as high as those in the case of aqueous electrolytes. They investigated the role of d-spacing on the overall electrochemical charge storage performance of the MXene electrodes employing different RTIL electrolytes for supercapacitor application and found that different chain lengths of alkylammonium (AA) cations -intercalated $Ti_3C_2T_x$ delivered higher capacitances, specific energy/power, and cycling stability than these earlier reported with the 1M EMIMTFSI/ACN and EMIMTFSI RTIL electrolytes, respectively. Therefore, optimal interlayer spacing (d-spacing) of different MXene-based electrodes can enhance the electrochemical performance in both organic and RTILs electrolytes with fast ion transport of high energy/power density, larger potential windows etc. by opening the door for high-performance energy storage devices [25].

5. Challenges and Future Outlook

Although pure MXenes and MXene-based electrode materials have already shown promising electrochemical energy storage performance with remarkable achievements through a wide variety of academic and industrial research and applications in energy storage devices, there is still a large body of development on the horizon. A number of challenges that are involved in the production of large-scale MXene-based materials with superior properties hinder their application in various types of batteries and supercapacitors. Namely, the main obstacles to the production of high-performance energy storage devices based on the MXene compounds belong:

- The stacking of the MXene single layers [103] limits the intercalation of cations and results in insufficient electrochemical performance.

One major issue is considerable high ionic diffusion resistance along the vertical direction arising from stacking MXenes' layers which significantly reduces the rate capability of MXene-based electrode materials at high current densities [110]. The structuring of the MXenes and formation of MXene-based hybrid materials is considered a promising solution for the enhancement of their electronic conductivity, stability and ion/electron

transfer [9]. The enlarged interlayer distances can provide fast diffusion of both ions and electrolytes, leading to superior electrochemical performance [34].

Therefore, further investigations shall be performed to find the balance between high-rate electrochemical performance and high-volume capacitance [100].

- The insufficient understanding of the surface termination effect on the MXene functional properties [35].

There is a considerable potential to manipulate the properties of the MXenes by optimization of their surface terminations [42], however, a systematical investigation shall be performed to establish the appropriate correlations.

- Non-safe processing methods for MXene-based materials production.

New safe, efficient and high-quality synthesis approaches shall be developed [20]. The availability and cost of MAX phase powders and the use of the large amount of intrinsic hazardous high concentrated HF are the major challenges for MXene production and these will continue to be the limiting factors for commercial development. A comprehensive effort is essential and desirable to address the environmental toxicity of MXene-based materials.

- Oxidation of MXene is related to the surface defects of MXene arising from the chemical etching process.

Removing the dissolved oxygen using dry nitrogen and storing MXenes at low temperatures could be a beneficial way to reduce the oxidation rate of MXenes. Thus, aggregation of the synthesized MXene and the influences of MXenes' structural characteristics such as basal spacing, surface chemistry, etc., have greatly affected the electrochemical charge storage mechanism of MXene-based electrode materials [111].

- A balance between the mechanical properties such as mechanical strength, toughness, flexibility etc. and the electrochemical properties of MXenes must be met and remains one of the major challenges for the fabrication of flexible supercapacitor devices.
- Issues for industrial production.

In the most of the research works, colloidal MXenes produced from solvent sonication or by employing long mixing/shaking times are used which do not display a desirable technique with industrial applicability. If the colloidal MXenes are not avoidable to achieve the so far realized and forecasted property improvements, then the industrial adoption of MXene into the electrodes of energy storage devices will face the same difficulties encountered with graphene. The high cost of MXene production must be lowered for industrial application and becomes one of the challenges for future research.

Despite the aforementioned challenges, owing to the several unique properties of MXene-based electrode materials, the future perspective of pure MXenes and MXene-based materials is brightly promising in energy storage and energy conversion fields but also various other fields such as in catalysis, environmental protection and biomedicine. Explicitly, for a better understanding of the electrochemical charge storage mechanism of MXene-based materials to obtain enhanced performances, substantial efforts, new ideas and the use of advanced research and investigation methods are essential.

Author Contributions: S.N.: writing—original manuscript preparation, review and editing; A.R.: writing—original manuscript preparation, review and editing, and B.S.: supervision, project administration, funding acquisition, validation, visualization, writing—review and editing. All authors have read and agreed to the published version of the manuscript.

Funding: This research received no external funding.

Data Availability Statement: Data sharing is not applicable to this article.

Conflicts of Interest: Authors declare that there is no conflict of interest for this publication.

References

1. Ansari, M.Z.; Seo, K.-M.; Kim, S.-H.; Ansari, S.A. Critical aspects of various techniques for synthesizing metal oxides and fabricating their composite-based supercapacitor electrodes: A review. *Nanomaterials* **2022**, *12*, 1873. [[CrossRef](#)] [[PubMed](#)]
2. Mateen, A.; Ansari, M.Z.; Hussain, I.; Eldin, S.M.; Albaqami, M.D.; Bahajaj, A.A.A.; Javed, M.S.; Peng, K.-Q. Ti₂CT_x-MXene aerogel based ultra-stable Zn-ion supercapacitor. *Compos. Commun.* **2023**, *38*, 101493. [[CrossRef](#)]
3. Hussain, I.; Lamiel, C.; Sahoo, S.; Ahmad, M.; Chen, X.; Javed, M.S.; Qin, N.; Gu, S.; Li, Y.; Nawaz, T.; et al. Factors affecting the growth formation of nanostructures and their impact on electrode materials: A systematic review. *Mater. Today Phys.* **2022**, *27*, 100844. [[CrossRef](#)]
4. Hussain, I.; Lamiel, C.; Javed, M.S.; Ahmad, M.; Chen, X.; Sahoo, S.; Ma, X.; Bajaber, M.A.; Ansari, M.Z.; Zhang, K. Earth- and marine-life-resembling nanostructures for electrochemical energy storage. *Chem. Eng. J.* **2023**, *454*, 140313. [[CrossRef](#)]
5. Kaskhedikar, N.A.; Maier, J. Lithium storage in carbon nanostructures. *Adv. Mater.* **2009**, *21*, 2664–2680. [[CrossRef](#)] [[PubMed](#)]
6. Yoo, E.; Kim, J.; Hson, E.; Zhou, H.-s.; Kudo, T.; Honm, I. Large reversible Li storage of graphene nanosheet families for use in rechargeable lithium ion batteries. *Nano Lett.* **2008**, *8*, 2277–2282. [[CrossRef](#)] [[PubMed](#)]
7. Liu, J.; Liu, X.W. Two-dimensional nanoarchitectures for lithium storage. *Adv. Mater.* **2012**, *24*, 4097–4711. [[CrossRef](#)]
8. Nan, J.; Guo, X.; Xiao, J.; Li, X.; Chen, W.; Wu, W.; Liu, H.; Wang, Y.; Wu, M.; Wang, G. Nanoengineering of 2D MXene-based materials for energy storage applications. *Small* **2021**, *17*, 1902085. [[CrossRef](#)]
9. Garg, R.; Agarwal, A.; Agarwal, M. A review on MXene for energy storage application: Effect of interlayer distance. *Mater. Res. Express* **2020**, *7*, 022001. [[CrossRef](#)]
10. Mateen, A.; Ansari, M.Z.; Abbas, Q.; Muneeb, A.; Hussain, A.; Eldin, E.; Alzahrani, F.M.; Alsaiari, N.S.; Ali, S.; Javed, M.S. In situ functionalization of 2D-Ti₃C₂T_x-MXenes for high-performance Zn-ion supercapacitor. *Molecules* **2022**, *27*, 7446. [[CrossRef](#)]
11. Liu, S.; Song, Z.; Jin, X.; Mao, R.; Zhang, T.; Hu, F. MXenes for metal-ion and metal-sulfur batteries: Synthesis, properties, and electrochemistry. *Mater. Rep. Energy* **2022**, *2*, 100077. [[CrossRef](#)]
12. Nitta, N.; Wu, F.; Lee, J.T.; Yushin, G. Li-ion battery materials: Present and future. *Mater. Today* **2015**, *18*, 252–264. [[CrossRef](#)]
13. Rakhi, R.B.; Bilal, A.; Hedhili, M.N.; Anjum, D.H.; Alshareef, H.N. Effect of postetch annealing gas composition on the structural and electrochemical properties of Ti₂CT_x MXene electrodes for supercapacitor applications. *Chem. Mater.* **2015**, *27*, 5314–5323. [[CrossRef](#)]
14. Chatterjee, S.; Ray, A.; Mandal, M.; Das, S.; Bhattacharya, S.K. Synthesis and characterization of CuO-NiO nanocomposites for electrochemical supercapacitors. *J. Mater. Eng. Perform.* **2020**, *29*, 8036–8048. [[CrossRef](#)]
15. Xu, X.; Yang, L.; Zheng, W.; Zhang, H.; Wu, F.; Tian, Z.; Zhang, P.; Sun, Z.M. MXenes with applications in supercapacitors and secondary batteries: A comprehensive review. *Mater. Rep. Energy* **2022**, *2*, 100080. [[CrossRef](#)]
16. Zhu, Q.; Li, J.; Simon, P.; Xu, B. Two-dimensional MXenes for electrochemical capacitor applications: Progress, challenges and perspectives. *Energy Storage Mater.* **2021**, *35*, 630–660. [[CrossRef](#)]
17. Li, X.; Wang, Y.; Zhao, Y.; Zhang, J.; Qu, L. Graphene materials for miniaturized energy harvest and storage devices. *Small Struct.* **2022**, *3*, 2100124. [[CrossRef](#)]
18. Miao, J.; Zhu, Q.; Li, K.; Zhang, P.; Zhao, Q.; Xu, B. Self-propagating fabrication of 3D porous MXene-rGO film electrode for high-performance supercapacitors. *J. Energy Chem.* **2021**, *52*, 243–250. [[CrossRef](#)]
19. Yang, L.; Zheng, W.; Zhang, P.; Chen, J.; Tian, W.B.; Zhang, Y.M.; Sun, Z.M. MXene/CNTs films prepared by electrophoretic deposition for supercapacitor electrodes. *J. Electroanal. Chem.* **2018**, *830–831*, 1–6. [[CrossRef](#)]
20. Jamil, F.; Ali, H.M.; Janjua, M.M. MXene based advanced materials for thermal energy storage: A recent review. *J. Energy Storage* **2021**, *35*, 102322. [[CrossRef](#)]
21. Anasori, B.; Lukatskaya, M.R.; Gogotsi, Y. 2D metal carbides and nitrides (MXenes) for energy storage. *Nat. Rev. Mater.* **2017**, *2*, 16098. [[CrossRef](#)]
22. Simon, P.; Gogotsi, Y.; Dunn, B. Where do batteries end and supercapacitors begin? *Science* **2014**, *343*, 1210–1211. [[CrossRef](#)]
23. Kim, E.; Song, J.; Song, T.-E.; Kim, H.; Kim, Y.-J.; Oh, Y.-W.; Jung, S.; Kang, I.S.; Gogotsi, Y.; Han, H.; et al. Scalable fabrication of MXene-based flexible micro-supercapacitor with outstanding volumetric capacitance. *Chem. Eng. J.* **2022**, *450*, 138456. [[CrossRef](#)]
24. Sohan, A.; Banoth, P.; Aleksandrova, M.; Nirmala, G.A.; Kollu, P. Review on MXene synthesis, properties, and recent research exploring electrode architecture for supercapacitor applications. *Int. J. Energy Res.* **2021**, *45*, 19746–19771. [[CrossRef](#)]
25. Liang, K.; Matsumoto, R.A.; Zhao, W.; Osti, N.C.; Popov, I.; Thapaliya, B.P.; Fleischmann, S.; Misra, S.; Prenger, K.; Tyagi, M.; et al. Engineering the interlayer spacing by pre-intercalation for high performance supercapacitor MXene electrodes in room temperature ionic liquid. *Adv. Funct. Mater.* **2021**, *31*, 2104007. [[CrossRef](#)]
26. Wang, K.; Wang, S.; Liu, J.; Guo, Y.; Mao, F.; Wu, H.; Zhang, Q. Fe-based coordination polymers as battery-type electrodes in semi-solid-state battery-supercapacitor hybrid devices. *ACS Appl. Mater. Interfaces* **2021**, *13*, 15315–15323. [[CrossRef](#)] [[PubMed](#)]
27. Ziegler, M.S. Evaluating and improving technologies for energy storage and backup power. *Joule* **2021**, *5*, 1925–1927. [[CrossRef](#)]
28. Lokhande, P.E.; Pakdel, A.; Pathan, H.M.; Kumar, D.; Vo, D.-V.N.; Al-Gheethi, A.; Sharma, A.; Goel, S.; Singh, P.P.; Lee, B.-K. Prospects of MXenes in energy storage applications. *Chemosphere* **2022**, *297*, 134225. [[CrossRef](#)]
29. Hart, J.L.; Hantanasirisakul, K.; Lang, A.C.; Anasori, B.; Pinto, D.; Pivak, Y.; van Omme, J.T.; May, S.J.; Gogotsi, Y.; Taheri, M.L. Control of MXenes' electronic properties through termination and intercalation. *Nat. Commun.* **2019**, *10*, 522. [[CrossRef](#)]
30. Naguib, M.; Halim, J.; Lu, J.; Cook, K.M.; Hultman, L.; Gogotsi, Y.; Barsoum, M.W. New two-dimensional Niobium and Vanadium carbides as promising materials for Li-ion batteries. *J. Am. Chem. Soc.* **2013**, *135*, 15966–16969. [[CrossRef](#)]

31. Zhan, C.; Naguib, M.; Lukatskaya, M.; Kent, P.R.C.; Gogotsi, Y.; Jiang, D. Understanding the MXene pseudocapacitance. *J. Phys. Chem. Lett.* **2018**, *9*, 1223–1228. [[CrossRef](#)]
32. Simon, P. Two-dimensional MXene with controlled interlayer spacing for electrochemical energy storage. *ACS Nano* **2017**, *11*, 2393–2396. [[CrossRef](#)] [[PubMed](#)]
33. Chen, Y.; Yang, H.; Han, Z.; Bo, Z.; Yan, J.; Cen, K.; Ostrikov, K.K. MXene-based electrodes for supercapacitor energy storage. *Energy Fuels* **2022**, *36*, 2390–2406. [[CrossRef](#)]
34. Long, M.Q.; Tang, K.K.; Xiao, J.; Li, J.Y.; Chen, J.; Gao, H.; Chen, W.H.; Liu, C.T.; Liu, H. Recent advances on MXene based materials for energy storage applications. *Mater. Today Sustain.* **2022**, *19*, 100163. [[CrossRef](#)]
35. Shinde, P.A.; Patil, A.M.; Lee, S.; Jung, E.; Jun, S.C. Two-dimensional MXenes for electrochemical energy storage applications. *J. Mater. Chem. A* **2022**, *10*, 1105. [[CrossRef](#)]
36. Sun, D.; Hu, Q.; Chen, J.; Zhang, X.; Wang, L.; Wu, Q.; Zhou, A. Structural transformation of MXene (V_2C , Cr_2C , and Ta_2C) with O groups during lithiation: A first-principles investigation. *Appl. Mater. Interfaces* **2016**, *8*, 74–81. [[CrossRef](#)]
37. Ghosh, M.; Ray, A.; Rao, G.M. Performance dependence of electrochemical capacitor on surface morphology for vertically aligned graphene nanosheets. *Ionics* **2020**, *26*, 981–990. [[CrossRef](#)]
38. Ray, A.; Roth, J.; Saruhan, B. Laser-induced interdigital structured graphene electrodes based flexible micro-supercapacitor for efficient peak energy storage. *Molecules* **2022**, *27*, 329. [[CrossRef](#)]
39. Ray, A.; Roy, A.; Ghosh, M.; Ramos-Ramón, J.A.; Saha, S.; Pal, U.; Bhattacharya, S.K.; Das, S. Study on charge storage mechanism in working electrodes fabricated by sol-gel derived spinel $NiMn_2O_4$ nanoparticles for supercapacitor application. *Appl. Surf. Sci.* **2019**, *463*, 513–525. [[CrossRef](#)]
40. Nguyen, T.K.; Aberoumand, S.; Dao, D.V. Advances in Si and SiC materials for high-performance supercapacitors toward integrated energy storage systems. *Small* **2021**, *17*, 2101775. [[CrossRef](#)]
41. Ibrahim, Y.; Mohamed, A.; Abdelgawad, A.M.; Eid, K.; Abdullah, A.M.; Elzatahry, A. The recent advances in the mechanical properties of self-standing two-dimensional MXene-based nanostructures: Deep insights into the supercapacitor. *Nanomaterials* **2020**, *10*, 1916. [[CrossRef](#)] [[PubMed](#)]
42. Wang, Y.; Xu, Y.; Hu, M.; Ling, H.; Zhu, X. MXenes: Focus on optical and electronic properties and corresponding applications. *Nanophotonics* **2020**, *9*, 1601–1620. [[CrossRef](#)]
43. Wang, C.; Chen, S.; Song, L. Tuning 2D MXenes by surface controlling and interlayer engineering: Methods, properties, and synchrotron radiation characterizations. *Adv. Sci. News* **2020**, *30*, 2000869.
44. Sugahara, A.; Yasunobu, A.; Satoshi, K.; Koji, Y.; Kazuma, G.; Minoru, O.; Masashi, O.; Atsuo, Y. Negative dielectric constant of water confined in nanosheets. *Nat. Commun.* **2019**, *10*, 850. [[CrossRef](#)]
45. Maleski, K.; Ren, C.E.; Zhao, M.Q.; Anasori, B.; Gogotsi, Y. Size-dependent physical and electrochemical properties of two-dimensional MXene flakes. *ACS Appl. Mater. Interfaces* **2018**, *10*, 24491–24498. [[CrossRef](#)] [[PubMed](#)]
46. Zhang, C.J.; Pinilla, S.; McEvoy, N.; Cullen, C.P.; Anasori, B.; Long, E.; Park, S.H.; Seral-Ascaso, A.; Shmeliov, A.; Krishnan, D.; et al. Oxidation stability of colloidal two-dimensional titanium carbides (MXenes). *Chem. Mater.* **2017**, *29*, 4848–4856. [[CrossRef](#)]
47. Huang, S.; Mochalin, V.N. Hydrolysis of 2D transition-metal carbides (MXenes) in colloidal solutions. *Inorg. Chem.* **2019**, *58*, 1958–1966. [[CrossRef](#)]
48. Naguib, M.; Come, J.; Dyatkin, B.; Presser, V.; Taberna, P.-L.; Simon, P.; Barsoum, M.W.; Gogotsi, Y. MXene: A promising transition metal carbide for lithium-ion batteries. *Electrochem. Commun.* **2012**, *16*, 61–64. [[CrossRef](#)]
49. Xie, Y.; Naguib, M.; Mochalin, V.N.; Barsoum, M.W.; Gogotsi, Y.; Yu, X.; Nam, K.-W.; Yang, X.-Q.; Kolesnikov, A.I.; Kent, P.R.C. Role of surface structure on Li-ion energy storage capacity of two-dimensional transition-metal carbides. *J. Am. Chem. Soc.* **2014**, *136*, 6385–6639. [[CrossRef](#)]
50. Luo, J.; Tao, X.; Zhang, J.; Xia, Y.; Huang, H.; Zhang, L.; Gan, Y.; Liang, C. Sn^{4+} ion decorated highly conductive Ti_3C_2 MXene: Promising lithium-ion anodes with enhanced volumetric capacity and cyclic performance. *ACS Nano* **2016**, *10*, 2491–2499. [[CrossRef](#)]
51. Ahmed, B.; Anjum, D.H.; Gogotsi, Y.; Alshareef, H.N. Atomic layer deposition of SnO_2 on MXene for Li-ion battery anodes. *Nano Energy* **2017**, *34*, 249–256. [[CrossRef](#)]
52. Zhang, C.; Kim, S.J.; Ghidui, M.; Zhao, M.-Q.; Barsoum, M.W.; Nicolosi, V.; Gogotsi, Y. Layered Orthorhombic $Nb_2O_5@Nb_4C_3T_x$ and $TiO_2@Ti_3C_2T_x$ hierarchical composites for high performance Li-ion batteries. *Adv. Funct. Mater.* **2016**, *26*, 4143–4151. [[CrossRef](#)]
53. Zou, G.; Zhang, Z.; Guo, J.; Liu, B.; Zhang, Q.; Fernandez, C.; Peng, Q. Synthesis of MXene/Ag composites for extraordinary long cycle lifetime storage at high rates. *ACS Appl. Mater. Interfaces* **2016**, *8*, 22280–22286. [[CrossRef](#)] [[PubMed](#)]
54. Jiang, T.; Yang, H.; Chen, G.Z. Enhanced performance of silicon negative electrodes composited with titanium carbide based MXenes for Lithium-ion batteries. *Nanoenergy Adv.* **2022**, *2*, 165–196. [[CrossRef](#)]
55. Li, X.; Chen, Z.; Li, A.; Yu, Y.; Chen, X.; Song, H. Three-dimensional hierarchical porous structures constructed by two-stage MXene-wrapped Si nanoparticles for Li-ion batteries. *Appl. Mater. Interfaces* **2020**, *12*, 48718–48728. [[CrossRef](#)] [[PubMed](#)]
56. Sobyra, T.B.; Matthews, K.; Mathis, T.S.; Gogotsi, Y.; Fenter, P. Operando X-ray reflectivity reveals the dynamical response of Ti_3C_2 MXene film structure during electrochemical cycling. *ACS Energy Lett.* **2022**, *7*, 3612–3617. [[CrossRef](#)]
57. Xia, Y.; Mathis, T.S.; Zhao, M.Q.; Anasori, B.; Dang, A.; Zhou, Z.; Cho, H.; Gogotsi, Y.; Yang, S. Thickness-independent capacitance of vertically aligned liquid-crystalline MXenes. *Nature* **2018**, *557*, 409–412. [[CrossRef](#)]

58. Zhou, J.; Zha, X.; Zhou, X.; Chen, F.; Gao, G.; Wang, S.; Shen, C.; Chen, T.; Zhi, C.; Eklund, P.; et al. Synthesis and electrochemical properties of two-dimensional Hafnium carbide. *ACS Nano* **2017**, *11*, 3841–3850. [CrossRef]
59. Wang, X.; Kajiyama, S.; Linuma, H.; Hosono, E.; Oro, S.; Moriguchi, I.; Okubo, M.; Yamada, A. Pseudocapacitnce of MXene nanosheets for high-powder sodium-ion hybrid capacitors. *Nat. Commun.* **2015**, *6*, 6544. [CrossRef]
60. Guo, X.; Gao, H.; Wang, S.; Yang, G.; Zhang, X.; Zhang, J.; Liu, H.; Wang, G. MXene-based aerogel anchored with antimony single atoms and quantum dots for high-performance potassium-ion batteries. *Nano Lett.* **2022**, *22*, 1225–1232. [CrossRef]
61. Yao, L.; Ju, S.; Yu, X. Rational surface engineering of MXene@N-doped hollow carbon dual-confined cobalt sulfides/selenides for advanced aluminum batteries. *J. Mater. Chem.* **2021**, *9*, 16878–16888. [CrossRef]
62. Zhu, J.; Zhang, X.; Gao, H.; Shao, Y.; Liu, Y.; Zhu, Y.; Zhang, J.; Li, L. VS₄ anchored on Ti₃C₂ MXene as a high-performance cathode material for magnesium ion battery. *J. Power Sources* **2022**, *518*, 230731. [CrossRef]
63. Qiu, S.Y.; Wang, C.; Jiang, Z.X.; Zhang, L.S.; Gu, L.L.; Wang, K.X.; Gao, J.; Zhu, X.D.; Wu, G. Rational design of MXene@TiO₂ nanoarray enabling dual lithium polysulfide chemisorption towards high-performance lithium-sulfur batteries. *Nanoscale* **2020**, *12*, 16678–16684. [CrossRef]
64. Bao, W.; Shuck, C.E.; Zhang, W.; Guo, X.; Gogotsi, Y.; Wang, G. Boosting performance of Na-S batteries using sulfur-doped Ti₃C₂T_x MXene nanosheets with a strong affinity to sodium polysulfides. *ACS Nano* **2019**, *13*, 11500–11509. [CrossRef] [PubMed]
65. Wang, Y.; Chen, R.; Chen, T.; Lv, H.; Zhu, G.; Ma, L.; Wang, C.; Jin, Z.; Liu, J. Emerging non-lithium batteries. *Energy Storage Mater.* **2016**, *4*, 103–129. [CrossRef]
66. Mashtalir, O.; Naguib, M.; Mochalin, V.N.; Dall’Agnese, Y.; Heon, M.; Barsoum, M.W.; Gogotsi, Y. Intercalation and delamination of layered carbides and carbonitrides. *Nat. Commun.* **2013**, *4*, 1716. [CrossRef]
67. Tang, Q.; Zhou, Z.; Shen, P. Are MXenes promising anode materials for Li ion batteries? Computational studies on electronic properties and Li storage capability of Ti₃C₂ and Ti₃C₂X₂ (X=F, OH) monolayer. *J. Am. Chem. Soc.* **2012**, *134*, 16909–16916. [CrossRef]
68. Ren, C.E.; Zhao, M.-Q.; Makaryan, T.; Halim, J.; Boota, M.; Kota, S.; Anasori, B.; Barsoum, M.W.; Gogotsi, Y. Porous two-dimensional transition metal carbide (MXene) flkaes for high-performance Li-ion storage. *ChemElectroChem* **2016**, *3*, 689–693. [CrossRef]
69. Liu, Y.-T.; Zhang, P.; Sun, N.; Anasoi, B.; Zhu, Q.-Z.; Liu, H.; Gogotsi, Y.; Xi, B. Self-assembly of transition metal oxide nanostructures on MXene nanosheets for fast and stable lithium storage. *Adv. Mater.* **2018**, *30*, 1707334. [CrossRef]
70. Wang, Y.; Li, Y.; Qiu, Z.; Wu, X.; Zhou, P.; Zhou, T.; Zhao, J.; Miao, Z.; Zhou, J.; Zhou, S. Fe₃O₄@Ti₂C₂ MXene hybrids with ultrahigh volumetric capacity as an anode material for lithium-ion batteries. *J. Mater. Chem. A* **2018**, *6*, 11189–11197. [CrossRef]
71. Li, X.; Zhu, J.; Fang, Y.; Lv, W.; Wang, F.; Liu, Y.; Liu, H. Hydrothermal preparation of CoO/Ti₃C₂ composite material for lithium-ion batteries with enhanced electrochemical performance. *J. Electroanal. Chem.* **2018**, *817*, 1–8. [CrossRef]
72. Tian, Y.; An, Y.; Feng, J. Flexible and freestanding silicon/MXene composite papers for high-performance lithium-ion batteries. *ACS Appl. Mater. Interfaces* **2019**, *11*, 10004–10011. [CrossRef]
73. Liang, X.; Garsuch, A.; Nazar, L.F. Sulfur cathodes based on conductive MXene nanosheets for high-performance Lithium-Sulfur batteries. *Angew. Chem. Int. Ed.* **2015**, *54*, 3907–3911. [CrossRef] [PubMed]
74. Huang, H.; Cui, J.; Liu, G.; Bi, R.; Zhang, L. Carbon-coated MoSe₂/MXene hybrid nanosheets for superior potassium storage. *ACS Nano* **2019**, *13*, 3448–3456. [CrossRef]
75. Nasrin, K.; Sudharshan, V.; Subramani, K.; Sathish, M. Insights into 2D/2D MXene heterostructures for improved synergy in structure toward next-generation supercapacitors: A review. *Adv. Funct. Mater.* **2022**, *32*, 2110267. [CrossRef]
76. Liu, F.; Wang, C.; Wang, L.; Huang, F.; Fan, J.; Shi, N.; Han, M.; Dai, Z. Oxygen-vacancy-rich NiMnZn-layered double hydroxide nanosheets married with Mo₂CT_x MXene for high-efficiency all-solid-state hybrid supercapacitors. *ACS Appl. Energy Mater.* **2022**, *5*, 3346–3358. [CrossRef]
77. Hong, Y.; Wang, Y.; Jing, Y.; Ma, J.; Du, C.-F.; Yan, Q. Surface modified MXene-based nanocomposites for electrochemical energy conversion and storage. *Small* **2019**, *15*, 1901503.
78. Chenya, R.; Zhu, D.; Qi, J.; Meng, Q.; Wei, F.; Ren, Y.; Sui, Y.; Zhang, H. MXene-modulated CoNi₂S₄ dendrite as enhanced electrode for hybrid supercapacitors. *Surf. Interfaces* **2021**, *25*, 101274.
79. Jie, X.; Yang, X.; Zou, Y.; Zhu, L.; Xu, F.; Sun, L.; Xiang, C.; Zhang, J. High density anchoring of NiMoS₄ on ultrathin Ti₃C₂ MXene assisted by dopamine for supercapacitor electrode materials. *J. Alloy. Compd.* **2022**, *891*, 161945.
80. Javed, M.S.; Zhang, X.; Ali, S.; Mateen, A.; Idrees, M.; Sajjad, M.; Batool, S.; Ahmad, A.; Imran, M.; Najam, T.; et al. Heterostructured bimetallic-sulfide layered Ti₃C₂T_x-MXene as a synergistic electrode to realize high-energy-density aqueous hybrid-supercapacitor. *Nano Energy* **2022**, *101*, 107624. [CrossRef]
81. Bao, S.; Li, L.; Chen, A.; Jen, T.-C.; Liu, X.; Shen, G. Continuous fabrication of Ti₃C₂T_x MXene-based braided coaxial zinc-ion hybrid supercapacitors with improved performance. *Nano-Micro Lett.* **2022**, *14*, 34.
82. Yun, J.; Echols, I.; Flouda, P.; Chen, Y.; Wang, S.; Zhao, X.; Holta, D.; Radovic, M.; Green, M.J.; Naraghi, M.; et al. Layer-by-layer assembly of reduced graphene oxide and MXene nanosheets for wire-shaped flexible supercapacitors. *ACS Appl. Mater. Interfaces* **2021**, *13*, 14068–14076. [CrossRef] [PubMed]
83. Venkateshalu, S.; Cherusseri, J.; Karnan, M.; Kumar, K.S.; Kollu, P.; Sathish, M.; Thomas, J.; Jeong, S.K.; Grace, A.N. New method for the synthesis of 2D vanadium nitride (MXene) and its application as a supercapacitor electrode. *ACS Omega* **2020**, *5*, 17983–17992. [CrossRef]

84. Nasrin, K.; Sudharshan, V.; Arunkumar, M.; Sathish, M. 2D/2D Nanoarchitected Nb₂C/Ti₃C₂ MXene heterointerface for high-energy supercapacitors with sustainable life cycle. *ACS Appl. Mater. Interfaces* **2022**, *14*, 21038–21049. [[CrossRef](#)]
85. Wei, Z.; Halim, J.; Rosen, J.; Barsoum, M.W. MXene-based symmetric supercapacitors with high voltage and high energy density. *Mater. Rep. Energy* **2022**, *2*, 100078.
86. Nasrin, K.; Sudharshan, V.; Subramani, K.; Karnan, M.; Sathish, M. In-situ synergistic 2D/2D MXene/BCN heterostructure for superlative energy density supercapacitor with super long life. *Small* **2022**, *18*, 2106051. [[CrossRef](#)] [[PubMed](#)]
87. Cai, C.; Wei, Z.; Deng, L.; Fu, Y. Temperature-invariant superelastic multifunctional MXene aerogels for high-performance photoresponsive supercapacitors and wearable strain sensors. *ACS Appl. Mater. Interfaces* **2021**, *13*, 54170–54184. [[CrossRef](#)]
88. Bai, Y.; Liu, C.; Chen, T.; Li, W.; Zheng, S.; Pi, Y.; Luo, Y.; Pang, H. MXene-copper/cobalt hybrids via Lewis acidic molten salts etching for high performance symmetric supercapacitors. *Angew. Chem.* **2021**, *133*, 25522–25526. [[CrossRef](#)]
89. Fan, Z.; Wang, J.; Kang, H.; Wang, Y.; Xie, Z.; Cheng, Z.; Liu, Y. A compact MXene film with folded structure for advanced supercapacitor electrode material. *ACS Appl. Energy Mater.* **2020**, *3*, 1811–1820. [[CrossRef](#)]
90. Liu, Y.; Zhou, H.; Zhou, W.; Meng, S.; Qi, C.; Liu, Z.; Kong, T. Biocompatible, high-performance, wet-adhesive, stretchable all-hydrogel supercapacitor implant based on PANI@rGO/Mxenes electrode and hydrogel electrolyte. *Adv. Energy Mater.* **2021**, *11*, 2101329. [[CrossRef](#)]
91. Wenxiang, C.; Fu, J.; Hu, H.; Ho, D. Interlayer structure engineering of MXene-based capacitor-type electrode for hybrid micro-supercapacitor toward battery-level energy density. *Adv. Sci.* **2021**, *8*, 2100775.
92. Huang, X.; Huang, J.; Yang, D.; Wu, P. A multi-scale structural engineering strategy for high-performance MXene hydrogel supercapacitor electrode. *Adv. Sci.* **2021**, *8*, 2101664. [[CrossRef](#)]
93. Kumar, S.; Rehman, M.A.; Lee, S.; Kim, M.; Hong, H.; Park, J.Y.; Seo, Y. Supercapacitors based on Ti₃C₂T_x MXene extracted from supernatant and current collectors passivated by CVD-graphene. *Sci. Rep.* **2021**, *11*, 649. [[CrossRef](#)]
94. Cho, S.; Kim, D.Y.; Seo, Y. Binder-free high-performance MXene supercapacitors fabricated by a simple electrospray deposition technique. *Adv. Mater. Interfaces* **2020**, *7*, 2000750. [[CrossRef](#)]
95. Ayman, I.; Rasheed, A.; Ajmal, S.; Rehman, A.; Ali, A.; Shakir, I.; Warsi, M.F. CoFe₂O₄ nanoparticle-decorated 2D MXene: A novel hybrid material for supercapacitor applications. *Energy Fuels* **2020**, *34*, 7622–7630. [[CrossRef](#)]
96. Guan, Y.; Jiang, S.; Cong, Y.; Wang, J.; Dong, Z.; Zhang, Q.; Yuan, G.; Li, Y.; Li, X. 2020. A hydrofluoric acid-free synthesis of 2D vanadium carbide (V₂C) MXene for supercapacitor electrodes. *2D Mater.* **2020**, *7*, 025010. [[CrossRef](#)]
97. Wang, X.; Mathis, T.S.; Sun, Y.; Tsai, W.Y.; Shpigel, N.; Shao, H.; Zhang, D.; Hantanasirisakul, K.; Malchik, F.; Balke, N.; et al. Titanium carbide MXene shows an electrochemical anomaly in water-in-salt electrolytes. *ACS Nano* **2021**, *15*, 15274–15284. [[CrossRef](#)]
98. Lukatskaya, M.R.; Kota, S.; Lin, Z.; Zhao, M.-Q.; Shpigel, N.; Levi, M.D.; Halim, J.; Taberna, P.-L.; Barsoum, M.W.; Simon, P.; et al. Ultra-highrate pseudocapacitive energy storage in two-dimensional transition metal carbides. *Nat. Energy Nat. Publ. Group* **2017**, *2*, 17105. [[CrossRef](#)]
99. Chen, J.; Chen, M.; Zhou, W.; Xu, X.; Liu, B.; Zhang, W.; Wong, C. Simplified synthesis of fluoride-free Ti₃C₂T_x via electrochemical etching toward high-performance electrochemical capacitors. *ACS Nano* **2022**, *16*, 2461–2470. [[CrossRef](#)]
100. Enyashin, A.N.; Ivanovski, A.L. Two-dimensional titanium carbonitrides and their hydroxylated derivatives: Structural, electronic properties and stability of MXenes Ti₃C_{2-x}N_x(OH)₂ from DFTB calculations. *J. Solid State Chem.* **2013**, *207*, 42–48. [[CrossRef](#)]
101. Xie, Y.; Kent, P.R.C. Hybrid density functional study of structural and electronic properties of functionalized Ti_{n+1}X_n (X=C, N) monolayers. *Phys. Rev. B* **2013**, *87*, 235441. [[CrossRef](#)]
102. Khazaei, M.; Ranjbar, A.; Arai, M.; Yunoki, S. Topological insulators in the ordered double transition metals M'₂M''C₂ MXenes (M'=Mo, W; M''=Ti, Zr, Hf). *Phys. Rev. B* **2016**, *94*, 125152. [[CrossRef](#)]
103. Sun, N.; Guan, Z.; Zhu, Q.; Anasori, B.; Gogotsi, Y.; Xu, B. Enhanced ionic accessibility of flexible MXene electrodes produced by natural sedimentation. *Nano-Micro Lett.* **2020**, *12*, 87–89. [[CrossRef](#)] [[PubMed](#)]
104. Wang, Y.; Wang, X.; Li, X.; Bai, Y.; Xiao, H.; Liu, Y.; Liu, R. Engineering 3D ion transport channels for flexible MXene films with superior capacitive performance. *Adv. Funct. Mater.* **2019**, *29*, 1900326. [[CrossRef](#)]
105. Wang, S.; Liu, Y.; Lu, K.; Cai, W.; Jie, Y.; Huang, F.; Li, X.; Cao, R.; Jian, S. Engineering rGO/MXene hybrid film as an anode host for stable sodium-metal batteries. *Energy Fuels* **2021**, *35*, 4587–4595. [[CrossRef](#)]
106. Lin, Z.; Sun, D.; Huang, Q.; Yang, J.; Barsoum, M.W.; Yan, X. Carbon nanofiber bridged two-dimensional titanium carbide as a superior anode for lithium-ion batteries. *J. Mater. Chem. A* **2015**, *3*, 14096–14100. [[CrossRef](#)]
107. Ray, A.; Saruhan, B. Application of ionic liquids for batteries and supercapacitors. *Materials* **2021**, *14*, 2942. [[CrossRef](#)] [[PubMed](#)]
108. Zhao, C.; Zheng, W. A review for aqueous electrochemical supercapacitors. *Front. Energy Res.* **2015**, *3*, 23. [[CrossRef](#)]
109. Lin, Z.; Daffos, B.; Taberna, P.-L.; Aken, K.L.V.; Anasori, B.; Gogotsi, Y.; Simon, P. Capacitance of Ti₃C₂T_x MXene in ionic liquid electrolyte. *J. Power Sources* **2016**, *326*, 575–579. [[CrossRef](#)]
110. Carey, M.; Barsoum, M.W. MXene polymer nanocomposites: A review. *Mater. Today Adv.* **2021**, *9*, 100120. [[CrossRef](#)]
111. Forouzandeh, P.; Pillai, S.C. MXenes-based nanocomposites for supercapacitor applications. *Curr. Opin. Chem. Eng.* **2021**, *33*, 100710. [[CrossRef](#)]

Disclaimer/Publisher's Note: The statements, opinions and data contained in all publications are solely those of the individual author(s) and contributor(s) and not of MDPI and/or the editor(s). MDPI and/or the editor(s) disclaim responsibility for any injury to people or property resulting from any ideas, methods, instructions or products referred to in the content.